An-Najah National University

Faculty of Graduate Studies

STRUCTURAL, ELECTRONIC, MAGNETIC, AND ELASTIC PROPERTIES OF THE FULL-HEUSLER COMPOUNDS: Fe_2MnIn, Au_2MnIn USING FP-LAPW METHOD

By

Salma Naser Darweesh Braik

Supervisors

Prof. Mohammed Abu-Jafar

Dr. Mahmoud Qarout

This Thesis is Submitted in Partial Fulfillment of the Requirements for the Degree of Master of Physics, Faculty of Graduate Studies, An-Najah National University, Nablus, Palestine.

2024

STRUCTURAL, ELECTRONIC, MAGNETIC, AND ELASTIC PROPERTIES OF THE FULL-HEUSLER COMPOUNDS: Fe_2MnIn, Au_2MnIn USING FP-LAPW METHOD

By
Salma Naser Darweesh Braik

This Thesis was Defended Successfully on 01/10/2024 and approved by

Prof. Mohammed Abu-Jafar	
Supervisor	Signature
Dr. Mahmoud Qarout	
Co-Supervisor	Signature
Prof. Jihad Asad	
External Examiner	Signature
Dr. Diana Dahliah	
Internal Examiner	Signature

Dedication

To my beloved parents and brothers who gave me endless love, encouragement, and everything to be the person who I am today.

To the person I chose to complete my life with, my husband Ahmad, thanks for being a supportive person and giving me all the motivation I need throughout this MSc. work.

To my cutest son Tayseer ALLAH bless him.

To my sincere professors.

To the memory of Prof. Issam Al-Ashqer may ALLAH have mercy on his soul.

To my dearest friends.

With love.

Acknowledgments

I would like to express my sincere gratitude to ALLAH, who gave me the patience, knowledge, and health to finish this MSc thesis, praise be to God.

In pursuant of Hadith of our prophet Mohammed peace be upon him" he who doesn't thank people, doesn't thank ALLAH". I would like to thank my dearest supervisors Prof. Mohammed Abu-Jafar and Dr. Mahmoud Farout for all support, help and valuable suggestions provided to me to finish this work successfully.

In the end, huge thanks to the faculty members of the physics department.

Declaration

I, the undersigned, declare that I submitted the thesis entitled:

STRUCTURAL, ELECTRONIC, MAGNETIC, AND ELASTIC PROPERTIES OF THE FULL-HEUSLER COMPOUNDS: Fe_2MnIn, Au_2MnIn USING FP-LAPW METHOD

I declare that the work provided in this thesis, unless otherwise referenced, is the researcher's own work, and has not been submitted elsewhere for any other degree or qualification.

Student's Name: _____

Signature: _____

Date: _____

List of Contents

List of Tables

List of Figures

List of Appendices

STRUCTURAL, ELECTRONIC, MAGNETIC, AND ELASTIC PROPERTIES OF THE FULL-HEUSLER COMPOUNDS: Fe_2MnIn, Au_2MnIn USING FP-LAPW METHOD

By
Salma Naser Darweesh Braik
Supervisors
Prof. Mohammed Abu-Jafar
Dr. Mahmoud Farout

Abstract

The structural, electronic, magnetic, and elastic characteristics of Fe_2MnIn and Au_2MnIn full Heusler alloys were analyzed in this study using the WIEN2k computational package.The full-potential linearized augmented plane wave (FP-LAPW) method, based on density functional theory (DFT), was implemented.

The generalized gradient approximation (GGA) was applied to the exchange-correlation potential (εxc) to derive the equilibrium structural parameters. To achieve more reliable band gap energy values, the modified Becke-Johnson (mBJ) potential was employed for enhanced numerical accuracy.

Magnetic property calculations indicate that both normal and inverse Fe_2MnIn and Au_2MnIn alloys exhibit ferromagnetic behavior. Normal Fe_2MnIn and inverse Au_2MnIn have been found to be mechanically unstable, whereas normal Au_2MnIn and inverse Fe_2MnIn are mechanically stable, both possessing ductility and ionic bonding traits.

Keywords: Full Heusler alloys, Ferromagnetic, Elastic, Electronic, FP-LAPW, DFT.

Chapter one

Introduction

1.1 History

Friedrich Heusler, a German chemist, discovered a series of ferromagnetic alloys in 1903, with the most important being those made of copper, manganese, and aluminum, thereby founding the field of Heusler alloys (1–4). These alloys are known for their remarkable magnetic properties at room temperature, a phenomenon that is surprising since they are composed of non-ferromagnetic elements (5).

After that, ferromagnetism was discovered in other alloys created from Cu and Mn but with several other elements, such as bismuth (Bi), tin (Sn), and strontium (Sb) (5). It was later revealed that this behavior was not unique to this particular alloy but extended to an entire class of similar alloys (5). Currently, more than a thousand Heusler alloys have been discovered. These materials, with stoichiometries of 1:1:1 or 2:1:1, are formed from diverse elemental combinations (6).

The phenomenon of ferromagnetism and the structure of the alloy that Heusler discovered were unknown in 1903, which made Heusler's work a significant discovery (5). The structural arrangement and elemental composition of Heusler alloys were not fully understood for an extended period.

Potter's 1929 study revealed that the elements in the Cu-Mn-Al system were arranged in an FCC superlattice, with X-ray techniques used for measurement (7).Using X-ray diffraction and anomalous-scattering techniques, Bradley and Rodgers conducted an in-depth investigation into the compositional and structural properties of Cu-Mn-Al materials (8).

The scientists' research demonstrated a correlation among the composition of a material, its atomic structure, and its magnetic behavior. Meticulous investigation showed that the coordination of two binary B2-type compounds (XY and XZ) produces Heusler alloys; a prime example is Fe_2MnIn, derived from FeMn and FeIn. This ability of the alloys to adopt the B2 configuration highlights their potential for the development of novel Heusler alloys (9)

1.2 Structure of Heusler alloys

Heusler alloys, a class of roughly 1,500 magnetic intermetallic compounds with varying properties, are distinguished by their face-centered cubic (FCC) crystal structure. This structural characteristic and the diversity of their properties have made them a significant focus of scientific research (4).

The classification of Heusler compounds is primarily crystal structure-based. Half-Heusler compounds have a C1b crystal structure with XYZ stoichiometry, while Full-Heusler compounds have a structure that can be called $L2_1$ and can be represented by the X_2YZ structure (10–12).

A key difference is that in Full-Heusler alloys, element X has a higher valence number than element Y, whereas in Half-Heusler alloys, the second X sublattice remains unoccupied.

Inverse Heusler alloys also follow the X_2YZ chemical representation (resembling Full-Heusler alloys but incorporating the C1b structural form). The fact that X and Y belong to the same period means that, in this case, X has fewer valence electrons than Y. The inverse Heusler alloy can be simply characterized as a Half-Heusler alloy with one extra X atom (13).

The chemical stoichiometry of Quaternary Heusler alloys (QHA) is XXYZ, and they adopt a Y-type crystalline structure (14).

Within these classifications, atoms X and Y in the structure denote d-block elements (transition metals), whereas Z represents a p-block element (main group element), as shown in the figure below.

Figure 1

Periodic table of Heusler alloys

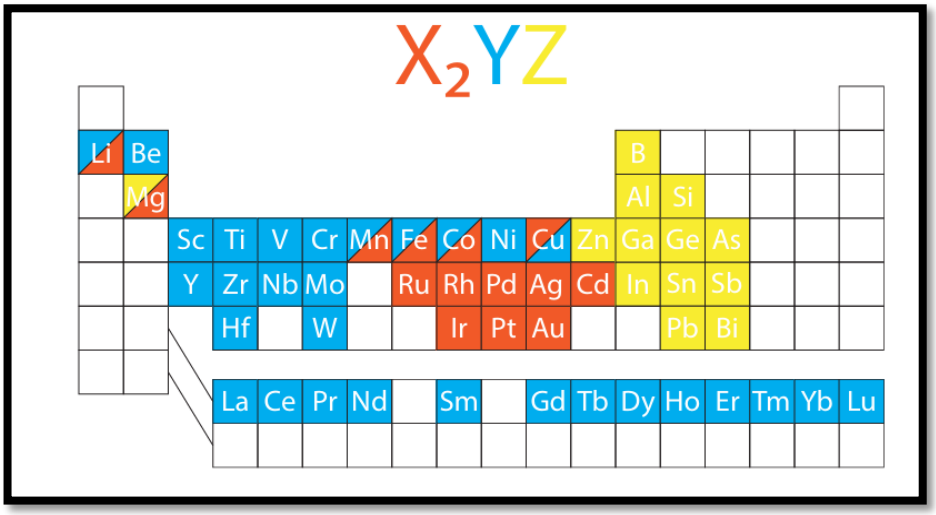

The Fm-3m (225) space group governs the atomic arrangement of regular Heusler compounds, with Wyckoff positions specifying the locations of X2 atoms at (0.25, 0.25, 0.25) and (0.75, 0.75, 0.75), Y atoms at (0.5, 0.5, 0.5), and Z atoms at the origin (12,15).

The atomic configuration of an inverse Heusler alloy, which crystallizes in the F-43m (216) space group, can be defined as: X2 atoms occupy (0.25, 0.25, 0.25) and (0.5, 0.5, 0.5), the Y element is situated at (0.75, 0.75, 0.75), and the Z atom is found at (0, 0, 0). Figure 2 below depicts the atomic arrangements in full, half, and inverse Heusler alloys (16).

Figure 2

The schematic Representation of the Crystal Lattice

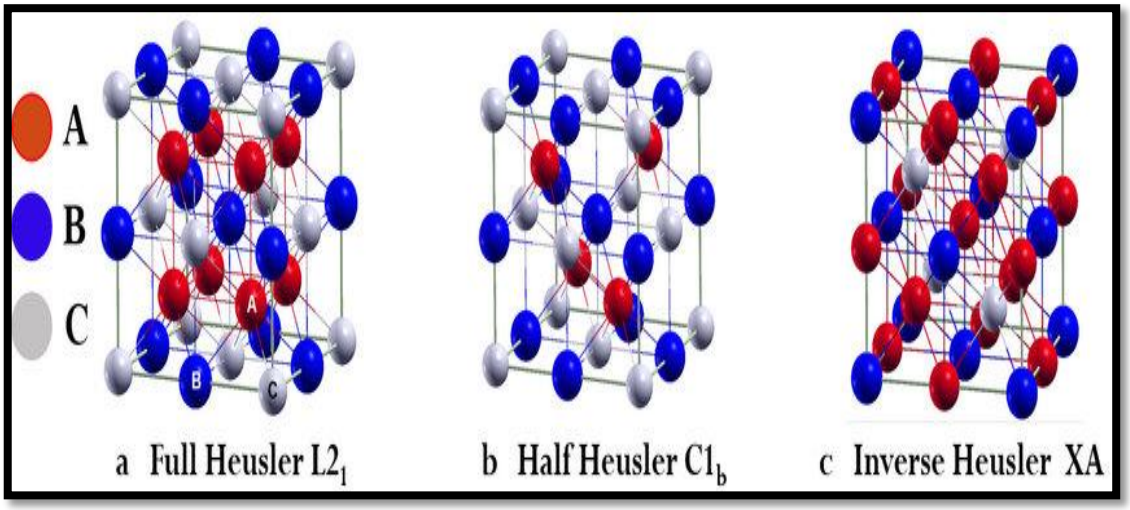

Note: (a) Full Heusler Alloy (b) Half Heusler Alloy, and (c) Inverse Heusler Alloy

In full Heusler alloys, the properties are largely dictated by the count of valence electrons. These electrons, found in the outermost shell of an atom, are critical for chemical bonding because they are less tightly held by the nucleus and can easily interact with other atoms to form bonds (17, 18).

Many Heusler alloys have lately been theoretically expected to be thermodynamically stable but haven't experimentally verified yet. Their lattice parameters commonly range from approximately 5.6 A to 7.2 A (19).

1.3 Literature Review

Numerous investigations have been conducted into Heusler alloys and their properties. Ferhat et al. (2010) employed the FP-LAPW method to investigate the structural, electronic, and magnetic properties of MBi alloys, where M represents Mn, V, and Cr (20). The Co_2FeGe Heusler compounds' structural, magnetic, and electronic behaviors were analyzed by Rai et al. (2012) through the Local Spin Density Approximation (LSDA) and the LSDA+U method, which applies a Hubbard U correction (21). Using the LSDA method, the crystal lattice constant, total magnetic moment, and bulk modulus were determined to be 5.758 Å, 5.391 μB, and 162.677 GPa, respectively. Conversely, in the LSDA+U case, the corresponding values were found to be 5.762 Å, 5.999 μB, and 144.684 GPa.

In 2014, Shao, Xiong et al. (22) used first-principles computational methods within the framework of density functional theory (DFT) with the generalized gradient approximation (GGA) to examine the mechanical, structural, and spin-polarized half-metallic properties of NiMnX (X = Sb, Si, As) and IrMnAs half-Heusler alloys.

In 2017, Amudhavalli et al. (23) used the Vienna Ab-initio Simulation Package (VASP) to study the structural, magnetic, mechanical, and electronic properties of half-Heusler materials AMnB, where B represents Ir, Au, Pt, Sn, or Sb.

The research confirmed that these six compounds remain stable in the α-phase. It was demonstrated that all six compounds are stable in the α-phase. The results of this research indicate that these six compounds are stable in the α-phase. The research has further revealed that these materials are metallic in nature under normal pressure conditions but are half-metallic in nature under pressure conditions. The elastic behavior

has confirmed that ionic bond alloys are mechanically stable under normal environmental conditions. Lastly, the magnetic behavior has confirmed that all half-Heusler alloy compounds studied are ferromagnetic in nature at atmospheric pressure. In 2017, through use of the FP-LAPW technique, Gupta et al. (24) studied the electronic structure, magnetic behavior, structural behavior, and other properties of Co_2VZ where Z = As and In. The calculated lattice parameters are 5.8 Å and 6.01 Å for Co_2VAs and Co_2VIn, respectively. The analysis of magnetic behavior verifies that both materials exhibit ferromagnetism and that each spin channel has energy gaps that enable their half-metallic behavior. In addition, it has been determined that these materials are brittle, incompressible and anisotropic and are stable. Their thermal and electrical conductance has been measured over a series of temperatures and pressures in regard to heat capacity.

Ahmed et al. (2017) (25) carried out a detailed examination of the electronic behavior, structural behavior, and thermoelectric behavior of half-Heusler materials ZMgN where Z = Li, Na and K. The calculated equilibrium lattice constants were found to be 4.9 Å and 5.32 Å and 5.82 Å for LiMgN and NaMgN and KMgN respectively as calculated by LDA and 5.01 Å and 5.45 Å and 6.01 Å by GGA. Calculations of electronic behavior have confirmed that LiMgN and NaMgN are direct band gap in nature while KMgN is indirect band gap in nature. The thermoelectric performance was studied by a series of parameters that included the figure of merit, power factor, electrical and thermal conductance, and Seebeck coefficient (S), thermal and electrical conductivity (σ), power factor (PF), and figure of merit (ZT) were measured to carry out the thermoelectric characterization over a temperature range.

In another research project in 2017, Wang et al. (26) studied a series of Heusler alloys with respect to rare earth elements like LuFeMnX with X as Al and Ga, YFeMnE with E as Al and Ga, LuCoCrR with R as Si and Ge, and LaCoCrAl and studied properties like half-metallic behavior, mechanical properties, magnetic properties, electronic structure, and structural properties.

In 2018, Abu Jafar et al. (27) studied $SrTMO_3$ with TM consisting of Rh and Zr through first-principles simulations based on density functional theory (DFT). In addition to that, Jain et al. (28) studied the magnetic behavior, electronic features, and optical features of Co_2TiZ Heusler alloys with Z as B, Al, In, and Ga in 2018 based on

DFT calculations with exchange-correlation functions (E_{xc}) under the scheme of Generalized Gradient Approximation. They calculated lattice parameters, values of energy bands, density of states (DOS), spin polarization, and bulk modulus values, and their findings labeled Co_2TiAl as half-metallic and identified Co_2TiB, Co_2TiGa, and Co_2TiIn as half-metallic under different pressure conditions. In conclusion, calculations were made in order to determine optical parameters like reflectivity, optical conductivity, and refractive index.

In 2018, a research by Fadila et al. (29) on full Heusler alloys Co_2XAl (where X is Fe and Ti) regarding their structural, mechanical, electronic, and magnetic properties. The research used the Full-Potential Linearized Augmented Plane Wave scheme with the WIEN2k code and used several exchange-correlation potentials. The calculated lattice parameters at equilibrium displayed outstanding agreement with both experimental and theoretical values. In terms of magnetic behavior, the use of Hubbard U potential in first-principles calculations corrected the underestimation of the total magnetic moment. Results obtained by utilizing mBJ and Generalized Gradient Approximation had outstanding correspondence with experimental data. Electronic properties' energy band gaps were optimized by utilizing mBJ-GGA and GGA+U approaches. Elastic constants were calculated through a numerical ab initio method. In the $L2_1$ phase, Co_2FeAl and Co_2TiAl were found to be stable under ambient pressure. Finally, the mechanical properties, including average longitudinal and transverse sound velocities as well as Debye temperatures, were reported.

Also in 2018, Mehmood et al. (30) studied the electronic, elastic, magnetic, and structural properties of RuMnZ half-Heusler alloys (Z = P, As) using the FP-LAPW method. Their findings revealed that the equilibrium lattice parameters ranged from 5.4 to 5.7 Å. Both compounds exhibited half-metallic behavior and ductile characteristics. Weak ferromagnetism was found in the magnetic property analysis, with total magnetic moments close to 1 μB. In contrast, the optical properties revealed metallic behavior, with elevated reflectivity, refractivity, and conductivity values.

The mechanical, electronic, magnetic, and half-metallic characteristics of CoCrY (Y = S, Te, Se) half-Heusler alloys were determined by Huang, Zhang et al. (31) in 2018 using first-principles computational methods within the GGA-DFT framework. Mokhtari, Dahmani, and colleagues (32) carried out a study in 2018 on ZVSb (Z = Fe,

Ni, Co) half-Heusler alloys, emphasizing their structural, electronic, and magnetic characteristics. They employed Density Functional Theory (DFT) calculations using the Generalized Gradient Approximation (GGA) and the Tran-Blaha modified Becke-Johnson (TB-mBJ) exchange-correlation functional.It was demonstrated that all six compounds are stable in the α-phase. The investigation later revealed that these materials have metallic behavior under normal pressure conditions; however, under enhanced pressure conditions, they have half-metallic behavior. A determination of the elastic properties revealed that the alloys are marked by ionic bonds and are mechanically stable under normal conditions. Additionally, a determination of the magnetic properties revealed that all half-Heusler alloy compounds are essentially magnetized at atmospheric pressure. In 2017, Gupta et al. used the FP-LAPW technique to analyze the electronic structure, magnetic properties, structural features, as well as thermoelectric, thermodynamics, and elastic properties of Co_2VZ with Z = As and In. The calculated lattice parameters of Co_2VAs and Co_2VIn were found to be 5.8 Å and 6.01 Å, respectively. The research on magnetic properties revealed that both materials are inherently ferromagnetic and that calculated energy gaps in both majority and minority spin channels supported their half-metallic behavior. Moreover, research findings illustrated that both materials are incompressible and anisotropic and are marked by stability, hardness, and brittleness. The observed heat capacity revealed diverse behavior under varying conditions of temperature and pressure as well as thermal and electrical conductance testing.

Ahmed et al. (2017) (25) carried out a detailed examination of the electronic behavior, structural behavior, and thermoelectric behavior of half-Heusler materials ZMgN where Z = Li, Na and K. The calculated equilibrium lattice constants were found to be 4.9 Å and 5.32 Å and 5.82 Å for LiMgN and NaMgN and KMgN respectively as calculated by LDA and 5.01 Å and 5.45 Å and 6.01 Å by GGA. Calculations of electronic behavior have confirmed that LiMgN and NaMgN are direct band gap in nature while KMgN is indirect band gap in nature. The thermoelectric performance was studied by a series of parameters that included the figure of merit, power factor, electrical and thermal conductance, and Seebeck coefficient (S), thermal and electrical conductivity (σ), power factor (PF), and figure of merit (ZT) over a temperature range provided thermoelectric characterization.

In another research project in 2017, Wang et al. (26) studied a series of Heusler alloys with respect to rare earth elements like LuFeMnX with X as Al and Ga, YFeMnE with E as Al and Ga, LuCoCrR with R as Si and Ge, and LaCoCrAl and studied properties like half-metallic behavior, mechanical properties, magnetic properties, electronic structure, and structural properties.

In 2018, Abu Jafar et al. (27) studied $SrTMO_3$ with TM consisting of Rh and Zr through first-principles simulations based on density functional theory (DFT). In addition to that, Jain et al. (28) studied the magnetic behavior, electronic features, and optical features of Co_2TiZ Heusler alloys with Z as B, Al, In, and Ga in 2018 based on DFT calculations with exchange-correlation functions (Exc) under the scheme of Generalized Gradient Approximation. They calculated lattice parameters, values of energy bands, density of states (DOS), spin polarization, and bulk modulus values, and their findings labeled Co_2TiAl as half-metallic and identified Co_2TiB, Co_2TiGa, and Co_2TiIn as half-metallic under different pressure conditions. In conclusion, calculations were made in order to determine optical parameters like reflectivity, optical conductivity, and refractive index.

In 2018, a research by Fadila et al. (29) on full Heusler alloys Co_2XAl (where X is Fe and Ti) regarding their structural, mechanical, electronic, and magnetic properties. The research used the Full-Potential Linearized Augmented Plane Wave scheme with the WIEN2k code and used several exchange-correlation potentials. The calculated lattice parameters at equilibrium displayed outstanding agreement with both experimental and theoretical values. In terms of magnetic behavior, the use of Hubbard U potential in first-principles calculations corrected the underestimation of the total magnetic moment. Results obtained by utilizing mBJ and Generalized Gradient Approximation had outstanding correspondence with experimental data. Electronic properties' energy band gaps were optimized by utilizing mBJ-GGA and GGA+U approaches. Elastic constants were calculated through a numerical ab initio method. In the $L2_1$ phase, Co_2FeAl and Co_2TiAl were found to be stable under ambient pressure. Finally, the mechanical properties, including average longitudinal and transverse sound velocities as well as Debye temperatures, were reported.

Also in 2018, Mehmood et al. (30) studied the electronic, elastic, magnetic, and structural properties of RuMnZ half-Heusler alloys (Z = P, As) using the FP-LAPW

method. Their findings revealed that the equilibrium lattice parameters ranged from 5.4 to 5.7 Å. Both compounds exhibited half-metallic behavior and ductile characteristics. Weak ferromagnetism was found in the magnetic property analysis, with total magnetic moments close to 1 μB. In contrast, the optical properties revealed metallic behavior, with elevated reflectivity, refractivity, and conductivity values.

The mechanical, electronic, magnetic, and half-metallic characteristics of CoCrY (Y = S, Te, Se) half-Heusler alloys were determined by Huang, Zhang et al. (31) in 2018 using first-principles computational methods within the GGA-DFT framework. Mokhtari, Dahmani, and colleagues (32) carried out a study in 2018 on ZVSb (Z = Fe, Ni, Co) half-Heusler alloys, emphasizing their structural, electronic, and magnetic characteristics. Their calculations employed Density Functional Theory (DFT) within the Generalized Gradient Approximation (GGA) framework, utilizing the Tran-Blaha modified Becke-Johnson (TB-mBJ) exchange-correlation functional. functional. It was demonstrated that all six compounds are stable in the α-phase.

The investigation later revealed that these materials have metallic behavior under normal pressure conditions; however, under enhanced pressure conditions, they have half-metallic behavior. A determination of the elastic properties revealed that the alloys are marked by ionic bonds and are mechanically stable under normal conditions. Additionally, a determination of the magnetic properties revealed that all half-Heusler alloy compounds are essentially magnetized at atmospheric pressure. In 2017, Gupta et al. used the FP-LAPW technique to analyze the electronic structure, magnetic properties, structural features, as well as thermoelectric, thermodynamics, and elastic properties of Co_2VZ with Z = As and In. The calculated lattice parameters of Co_2VAs and Co_2VIn were found to be 5.8 Å and 6.01 Å, respectively. The research on magnetic properties revealed that both materials are inherently ferromagnetic and that calculated energy gaps in both majority and minority spin channels supported their half-metallic behavior. Moreover, research findings illustrated that both materials are incompressible and anisotropic and are marked by stability, hardness, and brittleness. The observed heat capacity revealed diverse behavior under varying conditions of temperature and pressure as well as thermal and electrical conductance testing.

In the year 2017, Ahmed et al. (25) made a detailed examination of half-Heusler alloys ZMgN with Z standing for Li, Na, and K. Using FP-LAPW+lo and semiempirical

Boltzmann transport equations, they calculated lattice constants at equilibrium as 4.9 Å, 5.32 Å, and 5.82 Å under the Local Density Approximation (LDA) and 5.01 Å, 5.45 Å, and 6.01 Å under Generalized Gradient Approximation (GGA) for LiMgN, NaMgN, and KMgN. Their research revealed that LiMgN and NaMgN had a direct band gap and that KMgN had an indirect band gap. In addition, measurement of the Seebeck coefficient S, thermal and electrical conductance σ, power factor PF, and figure of merit ZT at a range of temperatures made it easy to characterize thermoelectric performance.

In another research project in 2017, Wang et al. (26) studied a series of Heusler alloys with respect to rare earth elements like LuFeMnX with X as Al and Ga, YFeMnE with E as Al and Ga, LuCoCrR with R as Si and Ge, and LaCoCrAl and studied properties like half-metallic behavior, mechanical properties, magnetic properties, electronic structure, and structural properties.

In 2018, Abu Jafar et al. (27) studied $SrTMO_3$ with TM consisting of Rh and Zr through first-principles simulations based on density functional theory (DFT). In addition to that, Jain et al. (28) studied the magnetic behavior, electronic features, and optical features of Co_2TiZ Heusler alloys with Z as B, Al, In, and Ga in 2018 based on DFT calculations with exchange-correlation functions (Exc) under the scheme of Generalized Gradient Approximation. They calculated lattice parameters, values of energy bands, density of states (DOS), spin polarization, and bulk modulus values, and their findings labeled Co_2TiAl as half-metallic and identified Co_2TiB, Co_2TiGa, and Co_2TiIn as half-metallic under different pressure conditions. In conclusion, calculations were made in order to determine optical parameters like reflectivity, optical conductivity, and refractive index.

In 2018, a research by Fadila et al. (29) on full Heusler alloys Co_2XAl (where X is Fe and Ti) regarding their structural, mechanical, electronic, and magnetic properties. The research used the Full-Potential Linearized Augmented Plane Wave scheme with the WIEN2k code and used several exchange-correlation potentials. The calculated lattice parameters at equilibrium displayed outstanding agreement with both experimental and theoretical values. In terms of magnetic behavior, the use of Hubbard U potential in first-principles calculations corrected the underestimation of the total magnetic moment. Results obtained by utilizing mBJ and Generalized Gradient Approximation had outstanding correspondence with experimental data. Electronic properties' energy band

gaps were optimized by utilizing mBJ-GGA and GGA+U approaches. Elastic constants were calculated through a numerical ab initio method. In the $L2_1$ phase, Co_2FeAl and Co_2TiAl were found to be stable under ambient pressure. Finally, the mechanical properties, including average longitudinal and transverse sound velocities as well as Debye temperatures, were reported.

Elastic constants were computed using a numerical ab initio approach. In the L21 phase, Co2FeAl and Co2TiAl were found to be stable under ambient pressure. Finally, the mechanical properties, including average, longitudinal, and transverse sound velocities, as well as Debye temperatures, were reported. Also in 2018, Mehmood et al. (30) studied the electronic, elastic, magnetic, and structural properties of RuMnZ half-Heusler alloys (Z = P, As) using the FP-LAPW method. Their findings revealed that the equilibrium lattice parameters ranged from 5.4 to 5.7 Å. Both compounds exhibited half-metallic behavior and ductile characteristics. Weak ferromagnetism was found in the magnetic property analysis, with total magnetic moments close to 1 μB. In contrast, the optical properties revealed metallic behavior, with elevated reflectivity, refractivity, and conductivity values. The mechanical, electronic, magnetic, and half-metallic characteristics of CoCrY (Y = S, Te, Se) half-Heusler alloys were determined by Huang, Zhang et al. (31) in 2018 using first-principles computational methods within the GGA-DFT framework. Mokhtari, Dahmani, and colleagues (32) carried out a study in 2018 on ZVSb (Z = Fe, Ni, Co) half-Heusler alloys, emphasizing their structural, electronic, and magnetic characteristics. Their calculations employed Density Functional Theory (DFT) within the Generalized Gradient Approximation (GGA) framework, utilizing the Tran-Blaha modified Becke-Johnson (TB-mBJ) exchange-correlation functional.

According to the results, the lattice parameters were 6.094 Å and 6.619 Å, the magnetic moments measured 1.9786 μB and 1.99 μB, and the band gaps were 1.430 eV and 0.641 eV, with elastic analysis ensuring mechanical stability.

EL Krimi et al. in 2020 carried out a research on Co_2CrAl as a full Heusler alloy with a focus on its structural, electronic, and magnetic properties. They used WIEN2k software in applying the FP-LAPW scheme in density functional theory (DFT) frameworks. They determined that the Fm-3m space group structure remains stable and calculated the optimized lattice constant, bulk modulus, and energy gap. The findings indicated

that Co_2CrAl maintains half-metallic behavior over a broad range of lattice parameters. The calculated potential indicated that the $L2_1$ phase exhibits greater stability in the ferromagnetic ground energy state compared to the paramagnetic state. The spin-related magnetic moments of Co and Cr were computed using the LSDA+U and GGA+U approaches.

Wakeel et al. (34) experimentally analyzed the structural characteristics and formation enthalpies of full Heusler alloys containing palladium (Pd) in 2021. They performed calculations on the structural parameters, band structures, and magnetic moments for Pd_2YZ, where Y represents Cu, Hf, Mn, Ti, and Zr, and Z stands for Al, Ga, In, and Sn. Their findings indicated that the lattice parameters matched the available data.

Furthermore, it was found that Pd-based Heusler alloys of various types had metallic behavior. The study has confirmed that Mn-based full Heusler alloys are ferromagnetic when compared to Pd full Heusler alloys made up of Zr, Hf, Ti, and Cu that have a mixed nature. Structural parameters such as lattice parameters, bulk modulus, first pressure derivatives, and the ratio of c to a were calculated by making use of the FP-LAPW scheme. The structural parameters optimized under Generalized Gradient Approximation for exchange-correlation potential and mBJ potential for energy gap calculations were used as a reference in research carried out by Yahya et al. in 2022 (35). In this research, it has been found that a prototypical Co_2CrAl Heusler alloy has half-metallic behavior in mBJ as well as in GGA calculations where a spin-down state has an energy gap.

Additionally, half-metallic behavior, characterized by an energy gap in the spin-down states, has been observed in both normal and inverse forms of Cr_2MnSb Heusler alloys, as well as in the tetragonal (139) Co_2CrAl and Cr_2MnSb alloys. The theoretical and experimental values reported in previous studies were found to align well with the computed total magnetic moments of both compounds. For the mechanical properties, the study found that both the normal and inverse forms of Co_2CrAl, as well as the normal Cr_2MnSb full-Heusler alloys, are stable; however, the inverse Cr_2MnSb exhibited instability in its ferromagnetic state.

In 2022, Belkilali et al. (36) investigated the structural, elastic, electronic, and optical properties of half-Heusler CaMgX compounds (X = Si, Ge, Pb, Sn, C) using the FP-

LAPW method within the DFT framework. A 2023 first-principles study by Jaradat et al. (37) examined the electronic, magnetic, and optical properties of NaS and NaSe alloys using DFT with the FP-LAPW method.

The exchange-correlation potential was treated with both the PBE-GGA and the mBJ-GGA approaches. Non-metallic character was observed for the spin-up configuration, while metallic behavior was observed for the spin-down orientation, based on electronic structure calculations.

Both the PBE-GGA and mBJ-GGA methods resulted in a total magnetic moment of 1.00 μB for these alloys. Optical analysis revealed a positive real part of the dielectric function, $\varepsilon_1(0)$, at zero energy in the spin-up channel, verifying the presence of an insulating phase. Oppositely, a highly negative $\varepsilon_1(0)$ was observed in the spin-down configuration, signifying metallic behavior. Moreover, the metallic characteristics were clearly evident in both components of the dielectric function as well as in the frequency-dependent refractive index, $n(\omega)$. Al-Masri et al. utilized the FP-LAPW technique in 2023 to investigate the structural, electronic, elastic, and magnetic behavior of Sc_2TiAl and Sc_2TiSi Heusler alloys.

The Sc_2TiAl Heusler alloy exhibited optimized lattice parameters of 6.88 Å and 6.84 Å in the normal and inverse configurations, respectively. Likewise, the Sc_2TiSi Heusler alloy had lattice parameters of 6.69 Å for the normal phase and 6.64 Å for the inverse phase. The total magnetic moments of both inverse and normal structures of Sc_2TiAl and Sc_2TiSi Heusler alloys were 2.86 μB, 2.09 μB, 2.97 μB, and 2.54 μB, respectively. In addition to this, a detailed analysis of their elastic properties was carried out and thereby their mechanical stability.

In 2024, AlShaikh et al. (39) performed a detailed investigation of the structural, electronic, magnetic, elastic, thermoelectric, dynamic, and optical properties of the CoCrTe half-Heusler alloy with the FP-LAPW method based on density functional theory (DFT). A modified Becke-Johnson potential was applied for better insight into the electronic band gap. The alloy was found to exhibit metallic characteristics. Its thermoelectric properties indicate that it has potential application in thermoelectric devices, with the status of mechanical and dynamic stability established by comprehensive examinations. In another study published in 2024, AlShaikh et al. (40)

used WIEN2k with the FP-LAPW method and DFT to study the CoCrSe half-Heusler alloy. The research concentrated on several physical properties, including structural, electronic, magnetic, elastic, thermoelectric, and dynamic features, with an emphasis placed on electronic aspects, such as band structure and density of states (DOS) plots. The mBJ exchange-correlation potential was used to precisely calculate the electronic energy bands. Also determined was magnetic moments while analysis of the spin-polarized electronic states offered deeper insight into the alloy's magnetic properties. This study evaluated the elastic properties and found that the CoCrSe alloy is mechanically and dynamically stable, although somewhat brittle and highly anisotropic. The researchers have also studied the thermoelectric features of this alloy yet again. In 2024, Abu-Jafar et al. (41) employed FP-LAPW coding in WIEN2k to study the structural, magnetic, electronic, elastic, and thermoelectric properties of the CoCrS half-Heusler alloy, improving the band gap calculation using the mBJ potential. They studied the electronic features, mainly focusing on band structure and density of states (DOS), while the magnetic features were discussed by means of the spin-polarized electronic state analyses.

1.4 Theoretical background

Our understanding of materials science and condensed matter physics has grown immensely. We have gained information regarding the dynamics of electrons and atoms that define solids in terms of material property theory. These physical properties are very much responsible for affecting behavior in our universe that ranges from atomic interactions to large-scale galaxy and planetary structure formation.

This section gives a detailed introduction to basic concepts and importance of physical properties in a wide range of scientific disciplines and everyday situations. Categorization and material analysis are based on critical factors that include their structural, electronic, magnetic, and elastic properties.

1.4.1 The Structural properties

The term "structural properties" refers to organization, arrangement, and relations at molecular and atomic levels of matter (42). In many environments, these properties play a central role in controlling material behavior and performance. The crystalline structure of matter refers to a systematic arrangement of molecules and atoms in a crystal lattice

and includes such things as atom positioning, dimensions of a unit cell, and lattice parameters.

Equations of state (EOS) that describe crystal structures define the connection between exterior conditions like pressure and temperature and structural properties of crystalline materials. The particular equation used in this calculation is expressed as follows.

The Murnaghan's equation of state

The energy-volume relationship expresses how a material's total energy changes with volume; it therefore allows an insight into the stability of those materials, their elasticity and other properties, under varying circumstances. Furthermore, the volume derivative of the energy-volume curve gives a chance to evaluate the bulk modulus and other elastic parameters. The equation of state according to Murnaghan is given as:

$$E(V) = E_0(V) + \frac{BV}{B'}\left[\frac{\left(\frac{V_0}{V}\right)^{B'}}{B'-1} + 1\right] - \frac{B\,V_0}{B'-1}. \qquad (1)$$

This framework defines that (V_0) is the equilibrium volume, (B) is the bulk modulus, and (B') is the variation rate of the bulk modulus. In addition, (E_0) is defined as the lowest energy level at absolute pressure and temperature.

The bulk modulus (B) and pressure (P) are related to each other as:

$$B' = \frac{dB}{dP}, where\ B = -V\frac{dP}{dV}. \qquad (2)$$

$$P = -\frac{dE}{dV}. \qquad (3)$$

This relationship is widely applied in condensed matter and materials science, especially in modeling elasticity and structural stability. It serves as a general theoretical background in understanding how materials respond to variations of pressure and temperature, usually combining experimental measurements and computational simulations to predict material behavior. While there are several equations of state to study the materials, the study at hand will focus on the Murnaghan equation of state.

1.4.2 Elastic properties

Before the role of the elastic properties becomes central in enabling a material's mechanical stability, the understanding of mechanical, dynamical, and thermodynamical stabilities must be mentioned (43). This part describes how one can assess the mechanical stability of our alloy based on crystalline defects by calculating the elastic constants. Dynamic stability of a material means that it will remain stable without any perturbation or revert back to stable form (44). Stability of a material in terms of thermodynamic is reached when the energy of the material does not reduce while an atomic arrangement is changed. This decrease of energy occurs mainly via one of two pathways: (1) Separation into some competing phases on the same average composition, or (2) Change into another crystal structure while keeping the same composition (45). The elastic properties of a given material allow us to evaluate the material in terms of stress or deformation, rigidity, mechanical behavior, and stability of structure (46). The elastic constants (Cij) are basic tools in defining a material's mechanical behavior. Their importance lies in their role in ensuring a material remains in a state of stability in a crystal structure when subjected to mechanical stress. Of utmost importance is that material elastic constants are responsible for protecting a material's crystal structure from damage when under stress. Conditions for mechanical stability are based on significant physical significance and are to be positive in value. The conditions for mechanical stability are formulated by the conditions as stated by (47):

$$C_{11}>0, \qquad C_{11}+2C_{12}>0, \qquad C_{11}-C_{12}>0, \qquad C_{44}>0$$

The mechanical properties of a solid are characterized by a number of important parameters. The bulk modulus (B) refers to resistance to isotropic compression, and shear modulus (S) refers to resistance to shape change. The effects of transverse strain are measured by means of Poisson’s ratio (v). In addition, the ratio B/S provides a measure to evaluate responses to both volumetric and shear stresses. Young’s modulus (Y) is a measure of tensile strength, and non-uniform factor (A) refers to non-uniform material properties.

1.4.3 Magnetic properties

The interaction of materials with external magnetic fields is characterized by their magnetic properties, which are influenced by the magnetic moments of their constituent atoms or ions.

The composition, structure and temperature of the material can affect these properties.

The magnetic moment (μ) represents the strength and orientation of a material's magnetic field that is created by the intrinsic rotation and orbital angular momentum of particles and is considered as a fundamental property of elementary materials, atoms, and particles(48).

A material's total magnetic moment is determined by adding up the magnetic moments of all its components.

The main magnetic properties include:

1. Magnetization: This describes how a material reacts to an external magnetic field, leading to magnetization, and is quantified as the magnetic moment per unit mass or volume (48).
2. Magnetic Susceptibility (χ): Measures how easily a material responds to an applied magnetic field so that it becomes magnetized, and it is very important in superconductors. It is expressed as the ratio of magnetization of a material to the strength of the applied magnetic field(48).
3. Permeability (μ): Describes how much the material allows magnetic field flow lines to pass through them easily. It denotes the capacity of a substance to produce an intrinsic magnetic field when exposed to an applied magnetics influence (48).
4. Retentivity: This refers to a material's capacity to retain its magnetization once the external magnetic field is removed. Materials with high retention capacity can remain magnetized even without an external field(48).
5. Coercivity: Quantifies the material's opposition to demagnetization. It expresses the strength of the reverse magnetic field required to completely demagnetize it after stimulation(48).

Types of Magnetic Behavior (49)

- **Ferromagnetism**

When the Mn atom is the one carrying the magnetic moment, as in X_2MnZ alloys, we can usually observe a value of approximately 4 μB.

Despite being metallic, Heusler alloys possess localized magnetic characteristics, making them a perfect choice for investigating the effects of atomic disorder and changes in electronic concentration (electron density) on magnetic properties.

Ferromagnetism in Heusler alloys remained unclear for many years and was finally understood after their electronic structure was discovered.

- **Anti-Ferromagnetism and Ferrimagnetism**

Anti-ferromagnetism behavior is more commonly observed in full Heusler alloys than in half Heusler alloys (when Y atom is carrying the 3d magnetic moment- mostly Mn atom), Because of the wider spacing between Mn atoms, X and Z atoms can minimize their interactions through shielding.

These magnetic properties are essential for a variety of applications, including magnetic storage devices, sensors, electric motors, transformers, and medical imaging (MRI). Understanding magnetic properties is also crucial in materials science, chemistry, and solid-state physics.

Some Heusler alloys have a unique property called half metallicity, this phenomenon occurs when one of the spin channels exhibits metallic behavior while the other demonstrates semiconductor-like behavior. This unique behavior facilitates impeccable spin polarization and an effective transfer of spin information.

1.4.4 Electronic properties

Characterizing the behavior of electrons within a material, including their energy levels, mobility, conductivity, and interactions with other particles or external forces, is the essence of electronic properties (50). These properties form a basis for predicting and controlling material performance in electronic devices.

Investigating the material’s energy band structure and the density of electronic states is crucial for understanding its electronic properties. The arrangement of electron energy levels, termed "bands," within a material's crystal lattice is described by the concept of band structure in condensed matter physics, and the properties of these bands are influenced by the momentum of the electrons (50).

Valence Band: This is the highest energy band. At the lowest possible temperature ($0^{o}K$), this band is fully occupied by electrons.

Conduction Band: is the empty band above the valence band at absolute zero temperature, and electrons can move to this band when excited allowing electrical conduction.

Fermi Energy: corresponds to the highest energy level occupied by electrons at absolute 0 Kelvin. Fermi Energy: is the highest energy level that electrons occupy at absolute zero temperature. DOS at Fermi energy is essential for investigating the electrical characteristics of materials, because it shows how electrons behave at the energy critical level for conduction.

Energy Band Gap: It defines the energy separation between the highest point of the valence band and the lowest point of the conduction band.

The difference between the energy of the top of the valence band and the bottom of the conduction band. The electrical conductivity of the material can be investigated through this factor:

Insulators: These materials exhibit an insulator characteristic when the band gap is greater than 3 ev.

Semiconductors: Materials with small band gap energy (greater than zero and less than 3 ev) are semiconductors.

In this material, electrons are able to move from the valence band to the conduction band, facilitating electrical conduction.

Metals: in metals there, there is an overlap between valence and conduction bands. Enabling continuous electron flow and high electrical conductivity.

Density of States (DOS): it describes the allocation of allowed electronic energy levels in a material.

It pertains to how many states are accessible for electrons at a particular energy level. The density of states usually reaches its maximum near the valence and conduction band edges.

Due to the overlap of the valence and conduction bands, metals have a high DOS across a wide energy range. In insulators and semiconductors, the DOS is zero within the band gap, meaning no electronic states exist there (50).

1.5 Applications

1.5.1 Spintronics

This study seeks to explore the structural, electronic, magnetic, and elastic attributes of Fe_2MnIn and Au_2MnIn, emphasizing their prospective roles in spintronics applications.

Researchers are striving to create devices endowed with unique features, including compact dimensions, reduced power usage, and enhanced computational capabilities for specific tasks beyond current limits (51).

They hope to learn and investigate something new about solid-state physics by understanding electron-spin behavior in materials (51).

Spintronics, short for spin electronics, is an emerging technological field with promising applications in next-generation nanoelectronic devices. It aims to reduce power consumption while enhancing memory and processing capabilities (52).

Spintronics investigates the intrinsic spin of electrons and their corresponding magnetic moments, in addition to their fundamental charge, within solid-state devices. Unlike classical electronics, it leverages electron spins as an extra degree of freedom, improving the efficiency of data storage and transfer (53).

The spin degree of freedom of electrons is harnessed by spintronics. In the 1960s, Leo Esaki's group at IBM conducted pioneering studies on controlling electrical current via electron spin, leading to the discovery of significant magnetoresistance in an antiferromagnetic EuSe barrier placed between metal electrodes (53).

Quantum semiconductor structures emerged as a result of progress in semiconductor thin film deposition, in particular molecular beam epitaxy. This progress also contributed to a broadening of research on magnetic multilayers (53).

The 1988 discovery of the giant magnetoresistance (GMR) effect, a consequence of this research, revolutionized magnetic sensor technology. This development later led to a very important step forward in areal density in hard disk drives. In the year 2007, Peter Grünberg and Albert Fert were both awarded jointly with a Nobel Prize for their trail-blazing work in Giant Magnetoresistance (GMR) (53).

In 2003, a first special issue of Proceedings of the IEEE on spintronics came out with the aim of recognizing progress made that year (53).

Since then, there has been rapid progress in spintronics, broadening its applications from nanoscale sensors that improve hard disk drive density to magnetic random-access memories (MRAM), which are increasingly considered potential alternatives to embedded flash, static random-access memory (SRAM), and eventually dynamic random-access memory (DRAM).

Devices that use spin current, coupled with the torque it generates, are being designed to create oscillators and enable data transmission without the need for conventional current (53).

Another application of the spin degree of freedom is the conversion of heat into energy using the spin Seebeck effect, enabling the control of quantum states in solids for data management and communication, as well as aiding in the understanding of biological computing systems (53).

The publication of this special issue on spintronics (53) follows recent developments in data storage, computing, communication, energy harvesting, and ultra-sensitive sensors.

One of the most important examples of spintronics is the GMR effect. It occurs in configurations where two ferromagnetic thin films are separated by a thin conductive layer. The magnetization of the ferromagnetic layers can be oriented either parallel or antiparallel (51).

Researchers discovered that they could utilize magnetoresistance (specifically "giant" magnetoresistance, due to the pronounced effect in this phenomenon) to create highly precise detectors for magnetic field variations, like those used in hard disk drives for data storage.

The read/write heads in question have achieved significant success in making possible the storage of gigabytes of digital data in networked hard drives in computers. Additionally, significant investments have been made in research and development in persistent memory devices using such materials, which can potentially form the basis for ultra-high-speed computers (51).

Contemporary researchers are working on two main strategies. One is to improve GMR technology using materials with a greater spin polarization, or, in a different approach, to optimize currently available devices to attain a better level of spin polarization (51).

The following approach emphasizes generating and regulating spin-polarized currents while investigating spin transport in semiconductors and their potential as spin-state polarizers and spin filters. If semiconductor-based spintronic devices could be developed, they might offer amplification, multi-functional capabilities, and easier integration with traditional semiconductor technology. However, difficulties remain, especially regarding the interaction of semiconductors with other materials and how to enable effective spin transport (51).

1.5.2 Magnetic shape memory

Categorized as smart or active substances, Magnetic Shape Memory (MSM) materials experience a shape alteration when exposed to magnetic fields under 1 T, returning to their original form when a spring force is applied or when the magnetic field is rotated by 90 degrees (54).

Motion and force may be generated when the deformation rate is approximately 10% (54).

Magnetic Shape Memory (MSM) materials are single-crystalline metal alloys that can convert electrical energy into mechanical energy and vice versa. They are typically composed of ferromagnetic elements like Mn, Ga, and Ni (54, 55).

The high magnetically induced strain and fast response times make MSM technology highly attractive for novel actuators in pneumatics, robotics, medical applications, and mechatronic devices (56).

The deformation of MSM alloys can alter their magnetic properties an accompanying phenomenon that occurs concurrently with actuation. This effect is advantageous for designing sensors to measure displacement, speed, or force, as well as for developing devices that harvest mechanical energy (57).

Characterized by a tetragonal structure in its unit cells, the martensite phase of the alloy emerges at low temperatures. However, upon heating beyond the martensite–austenite transition temperature, the alloy shifts to the austenite phase, where the unit cells take on a cubic form, eliminating the magnetic shape memory effect (57).

1.5.3 Topological insulators

The nature of topological insulators allows them to exhibit two different behavioral traits simultaneously.

Their interior behaves like an insulator, while their surface behaves like a conductor, which means that electrons can only move along the material's surface (58).

These materials possess a distinct energy band gap separating the valence and conduction bands, distinguishing topological insulators from conventional insulators (59).

"Twisting" means that the energy band gap of topological insulators cannot be deformed into that of an ordinary insulator without closing the gap, which would form a conducting band (60).

We can say that a topological insulator is an insulator that cannot be turned into an ordinary insulator without passing through a transient conducting state (60).

This means that topological insulators and ordinary insulators occupy discrete regions in the phase diagram, linked only by conducting states.

Accordingly, topological insulators provide an instance of a state of matter unexplained by the Landau symmetry-breaking theory, which describes ordinary states of matter (58).

1.6 Study Gap

It is noteworthy that there exists a gap in the existing body of research concerning these two compounds (Fe_2MnIn and Au_2MnIn).

To the best of our knowledge, no one has studied the electronic and elastic properties of Fe_2MnIn and Au_2MnIn in their normal configurations, nor has any study explored any type of properties for these compounds in their inverse configurations. Additionally, no one has studied both compounds in both configurations using the FP-LAPW method.

In their paper in 2019, Aguilera-Granja et al. performed a study with sixty Heusler compounds, such as Fe_2MnIn and Au_2MnIn, using the SIESTA code. The calculated lattice parameters were established to be 6.197 Å for Fe_2MnIn and 6.726 Å for Au_2MnIn, while calculated total magnetic moments were established to be 7.86 μB and 4.09 μB, respectively.

This study seeks to identify the elastic, magnetic, electronic, and structural properties of normal and inverse Fe_2MnIn and Au_2MnIn cubic Heusler full alloys. This study has importance due to the possible applications in physics, especially in the field of spintronics.

This research utilized the FP-LAPW approach to study electronic, structural, elastic, and magnetic properties in Fe_2MnIn and Au_2MnIn full Heusler alloys in both normal and inverted configurations.

The first chapter covers the concept of Heusler alloys, their various types, applications, and pertinent previous studies. In the second chapter, the methodology is presented. Chapter 3 discusses the calculations and results. Finally, in Chapter 4, the conclusion is summarized.

Chapter Two

Methodology

Solid-state materials contain unit cells with numerous atoms arranged at defined positions, made up of substantial positively charged nuclei and smaller negatively charged electrons. These atoms exhibit repetition with periodic boundary conditions, presenting theorists with many-body problems. Nevertheless, the intrinsic **lightness** of particles introduces a quantum many-body problem (61).

The Hamiltonian describing the many-body problem is expressed as follows:

$$\widehat{H} = -\frac{\hbar^2}{2}\sum_{i=1}^{N}\frac{\nabla^2\vec{R}_i}{M_i} - \frac{\hbar^2}{2}\sum_{i=1}^{N}\frac{\nabla^2\vec{r}_i}{m_e} - \frac{1}{4\pi\epsilon_0}\sum_{ij}^{N}\frac{e^2Z_i}{|\vec{R}_i-\vec{r}_i|} + \frac{1}{8\pi\epsilon_0}\sum_{i\neq j}^{N}\frac{e^2}{|\vec{r}_i-\vec{r}_j|} + \frac{1}{8\pi\epsilon_0}\sum_{i\neq j}^{N}\frac{e^2Z_iZ_j}{|\vec{R}_i-\vec{R}_j|} \quad . \qquad (4)$$

Where e is the elementary charge,

Z_iZ_j are the atomic numbers of i_{th} and j_{th} particles, respectively.

Planck's constant is written as h

Δ = is the Laplacian,

The nuclei's mass is denoted by M,

me is the mass of the electron,

ϵ_0 is the vacuum permittivity,

$\vec{R}_i$ is the radius of the i_{th} nuclei,

$\vec{r}_i$ specifies the radius of the *i*th electron.

$\vec{R}_i - \vec{r}_i$ is the distance from the i_{th} nucleus to the i_{th} electron.

In equation (1), the initial two terms represent the kinetic energy operator for the n_{th} nuclei (T_n), and for the electrons (T_e), respectively.

The Coulomb interactions are specified by the final three terms: V_{en} represents the force between nuclei and electrons, V_{ee} denotes the repulsion among electrons, and V_{nn} indicates the nuclear interplay, in that order.

Some approximations are used to solve it:

2.1 Born-Oppenheimer Approximation

In the Born-Oppenheimer approach, independence is assumed between the motion exhibited by electrons and that displayed by nuclei. This stems from the substantial difference in mass, with electrons being significantly lighter and moving at much higher speeds than nuclei. Consequently, it is feasible to presume that electrons are in instantaneous equilibrium with the stationary nuclei(61).

When this approximation is applied, it results in a group of N-Z negatively charged particles that interact and move under the influence of the fixed nuclear potential (source of positive charges), due to that, the first term T_n will be neglected, and the last term V_{nn} becames constant.

Thus, the many-body problem can be expressed as:

$$H = T_e + V_{ee} + V_{nn} + V_{en}\,. \qquad (5)$$

Where the sum of last two terms called the external potential V_{ext}.

The problem became simpler, but still hard to solve.

2.2 Hartree and Hartree-Fock Approximation

The Hartree approximation suggests that the solution to a many-body problem can be modeled using the product of wave functions corresponding to individual particles. In this context, each particle is presumed to move independently of other particles (62).

The wave function describing the behavior of electrons can be formulated as follows:

$$\Psi\,(r_1, r_2, r_3 \ldots r_N) = \Psi_1(r_1)\Psi_2(r_2)\Psi_3(r_3)\ldots\Psi_N(r_N), \qquad (6)$$

where the $\Psi_N(r_N)$ is the wave function for the electrons.

To describe systems independent of time, the Schrödinger equation is presented as:

$$\sum (T_S + V_{ext} + V_H)\Psi(r_n) = E\,\Psi(r_n), \qquad (7)$$

here, T_S represents the single-electron kinetic energy, V_{ext} denotes the external potential, and V_H stands for the Hartree potential applicable to non-interacting fermions. The expression for V_H can be formulated as:

$$\widehat{V_H} = \frac{1}{8\pi\varepsilon_0}\sum_{ij}^{N}\frac{|\psi(r_i)|^2|\psi(r_j)|^2 d^3r_i d^3r_j}{|\vec{r_i}-\vec{r_j}|}. \quad (8)$$

In this approximation, we assumed that we have a system of non-interacting electrons, so that we have a probability of finding two electrons at the same point in space.

This potential is good for many electron systems, but for semiconductors, especially for accurate electronic structure calculations, it's not accurate and has some limitations. So, here we need to use other approximations to get accurate results.

The Hartree-Fock approximation takes into account the wave function's anti-symmetry, a consequence of the exclusion principle formulated by Pauli, which prohibits the simultaneous occupation of the same quantum state by two identical electrons.

2.3 Density Functional Theory (DFT)

In physics and chemistry, Density Functional Theory (DFT) serves as a key method for addressing the electronic structure of many-body problems. It's a widely utilized method in condensed matter physics, computational physics and chemistry, because of its efficiency to handle a large number of electrons with complete precision. particularly in large molecules or solids, by transforming it into a single-body problem.

This approach is widely utilized in condensed matter physics, computational physics, and chemistry because of its exceptional ability to manage large electron systems with great accuracy. The ground state density, denoted as ρ_0, is generated by minimizing the energy functional (63).

Thus, E(ρ) is defined as the sum of the Hartree energy and the exchange-correlation functional E, which is an unknown functional (64).

$$E(\rho) = T_s(\rho) + E_c(\rho) + E_{ii}(\rho) + E_{xc}(\rho) + E_H(\rho)\ , \quad (9)$$

Where $E(\rho)$ is the energy dependent on electron density, and the initial term Ts represents the single kinetic energy, the second term E_c denotes the Coulomb energy between nuclei and electrons, whereas $E_{ii}(\rho)$ signifies the interaction between nuclei.

The unidentified part E_{xc} which equals $E_x + E_c$ represents the exchange-correlation energy, in this framework, Ex is associated with the Pauli exclusion principle, Ec emerges from the interaction of spin with electrons, and EH represents the Hartree potential, described as:

$$E_H(\rho) = \frac{e^2}{2}\int \; d^3r\, d^3r' \; \frac{\rho(\vec{r})\rho(\vec{r})}{|\vec{r}-\vec{r}|}. \qquad (10)$$

A single-particle Schrodinger equation (Kohn-Sham equation) according to the variational principle is given by (61):

$$\left[T_S \; + V_{ext}(r) + V_H\big(\rho(r)\big) + V_{XC}\big(\rho(r)\big)\right]\Phi_i(r) = \; \varepsilon_i\Phi_i(r)\,, \qquad (11)$$

The right-hand side of equation (8) consists of εi, representing the energy of a single particle, the electron wave function Φi, as well as VH (the Hartree potential), $Vext$ (the Coulomb potential), and VXC (the exchange-correlation potential).

2.4 Single particle Kohn-Sham Equation

In DFT, the Kohn-Sham equation acts as a cornerstone for detailing the electronic structure and behavior of materials. The single-particle Kohn-Sham frameworks are utilized to compute the electron density and energy of the system.

This method is based on the idea of an imaginary system of non-interacting electrons, which produces an electron density matching that of the real system, thereby simplifying the many-body problem into a more tractable single-particle framework (61).

These equations are solved self-consistently until a converged solution is obtained as illustrated in Figure 3 below.

Figure 3

Illustrates a flowchart depicting the n^{th} iteration in solving the Kohn-Sham equation through a self-consistent procedure

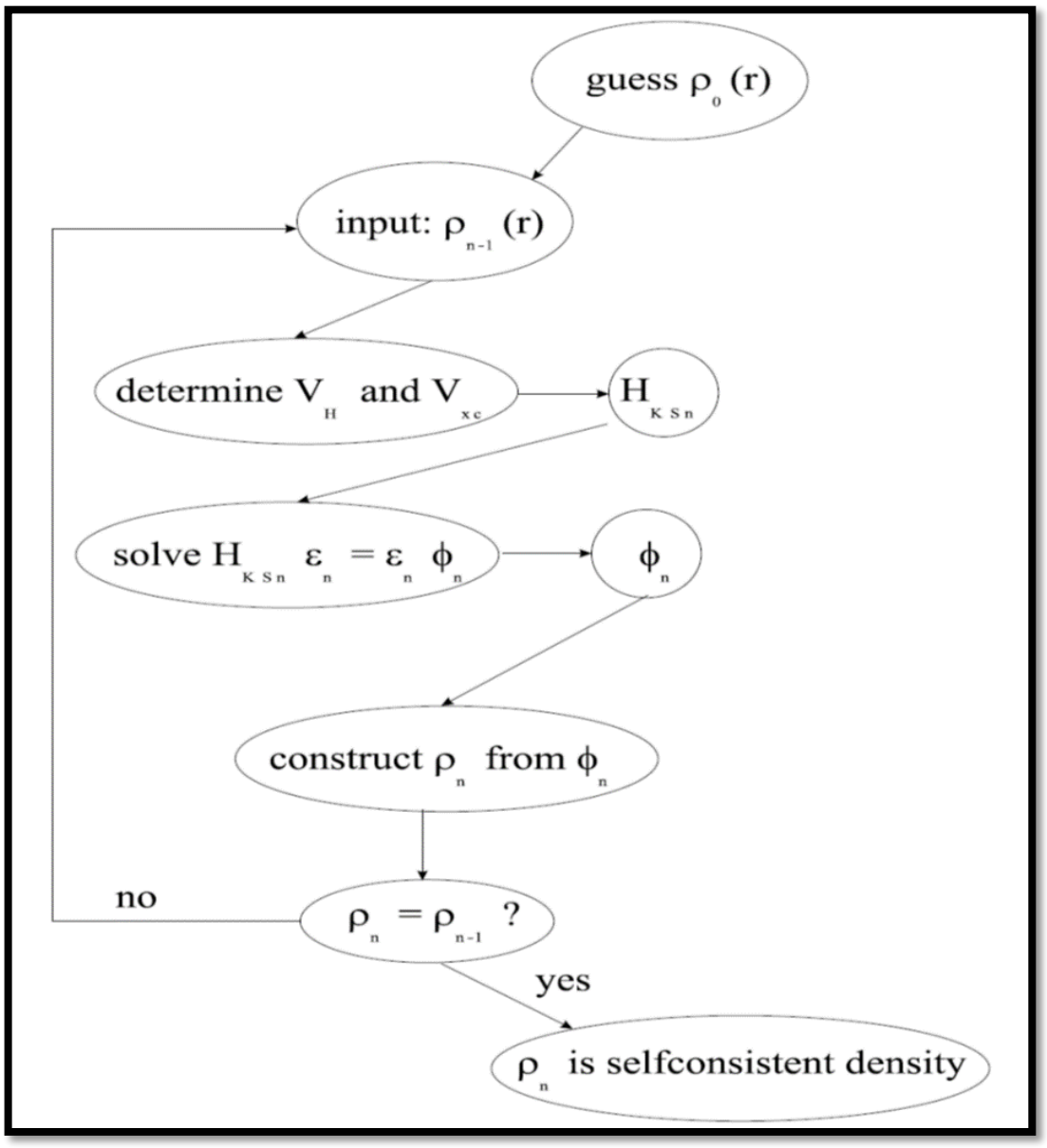

In Figure 3, an initial estimate of the electron density is conjectured, and a Kohn-Sham Hamiltonian (H_{KS1}) is formulated accordingly. Kohn-Sham equations solved, the new electron density is obtained from the wave function, finally by comparing the new density with the initial one, if the two values are equal then the solution is completed, and if they are not equal then the new density will be used as an initial density and the steps will be repeated until the solution converges (61).

2.5 The Exchange-correlation Functional

The exchange-correlation functional remains unknown, yet it is necessary to proceed despite this limitation.

The Exchange-Correlation functional relies on the application of the Generalized Gradient Approximation (GGA) and Local Density Approximation (LDA) for its proper formulation (61).

2.6 Local Density Approximation (LDA)

The Local Density Approximation (LDA) is a highly effective method within Density Functional Theory (DFT), frequently employed to compute the exchange-correlation term. This method is particularly useful in describing short-range interactions with good accuracy. A major drawback to Local Density Approximation (LDA) is that it cannot satisfactorily describe the varied set of long-range exchange-correlation interactions with adequate accuracy, particularly those for Van der Waals forces.

The Local Density Approximation is incorporated in Kohn-Sham formulation, as defined in the framework of Density Functional Theory. By Hohenberg-Kohn theorem, ground state energy for an electron system is given in a specific form with respect to electron density and, in a similar manner, the exchange-correlation energy is given as a functional of electron density (61).

It is important to point out that the exchange-correlation functional cannot be precisely determined and thus has to be estimated.The Exchange-Correlation Functional is defined as follows:

$$E_{xc}^{LDA} = \int \rho(\vec{r})\varepsilon_{xc}[\rho(\vec{r})]d\vec{r} \qquad (12)$$

The function ε_{xc} represents the Exchange-Correlation energy per electron in an infinite homogeneous electron gas with density (r).

The formula shows that the exchange-correlation for density ρ(r) can be computed by partitioning the system into small, localized regions of uniform density.

This suggests the validity of this approximation when the electron density exhibits very slowly gradual variations with position.

The function ε_{xc} can be expressed as a summation of exchange and correlation contributions (65),

$$\varepsilon_{xc} = \varepsilon_x + \varepsilon_c \ . \quad (13)$$

The initial and secondary contributions arise from the Pauli exclusion principle and the interaction between fermions electrons sharing the same spin, respectively.

Furthermore, the main point that makes this system simpler to solve than, for example, Hartree-Fock equations, is that the efficient possibility is local.

2.7 Generalized Gradient Approximation (GGA)

The Generalized Gradient Approximation (GGA) offers a more refined technique than the Local Density Approximation (LDA), as it considers the exchange-correlation energy to be a function of the electron density at every point in space (66).

Unlike other approaches, this method integrates the electron density gradient to enhance the accuracy of the exchange-correlation energy calculation (67).

$$E_{xc}^{GGA} = \int \rho(\vec{r})\varepsilon_{xc}[\rho(\vec{r}), \vec{\nabla}\rho(\vec{r})]d\vec{r} \ . \quad (14)$$

2.8 The Modified Becke-Johnson (mBJ) Potential

In density functional theory computations, the revised Becke-Johnson potential functions as a tailored exchange potential, improving the energy band gap for semiconductors and insulators (68).

2.9 Augmented Plane Wave (APW) Method

To address the Kohn-Sham equation, the enhanced plane wave technique is utilized, treating electrons distant from nuclei as nearly free and representing them with plane waves, whereas those near nuclei are modeled with atomic-like functions due to their free-atom-like behavior (61).

As a result, space is segmented into two separate areas: the muffin-tin domain and the interstitial zone. The first one encompasses the space occupied by muffin-tin spheres drawn around each atom, while the second one constitutes the remaining space outside these spheres (61).

The wave function ψn is characterized as follows:

$$\phi_{\vec{K}}^{\vec{k}}(\vec{r},E) = \begin{cases} \frac{1}{\sqrt{V}} e^{i(\vec{k}+\vec{K}).\vec{r}} & \vec{r} \in I \\ \sum_{l,m} A_{lm}^{\alpha,\vec{k}+\vec{K}} u_l^{\alpha}(r',E) Y_m^l(\hat{r}') & r' < S_{\alpha} \end{cases} . \quad (15)$$

The radial portion is denoted by $u_l^{\alpha}(r',E)$ in this context.

$Y_m^l(\hat{r}')$ is the spherical harmonics,

Within this framework, $\overrightarrow{k}$, $\overrightarrow{k}$ and $\vec{r}$ symbolize the wave vector associated with the irreducible Brillouin Zone, while V indicates the unit cell's volume.

Figure 4

Spatial Regions of the APW Method

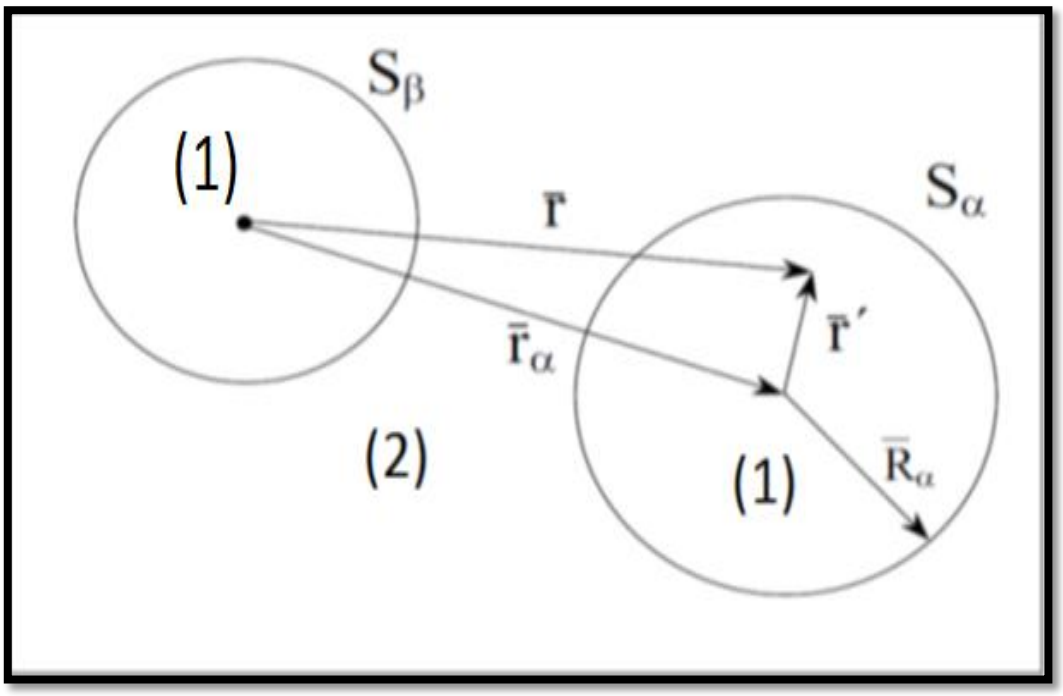

Note: (1) Muffin-Tin and (2) Interstitial Zones

2.10 The Linearized Augmented Plane Wave (LAPW) Method

The problem with the APW method is that: $u_l^{\alpha}(r', E)$ have to be constructed at the eigenenergy E of the searched eigenstate. This problem is solved in LAPW method by expanding u_l^{α} using Taylor expansion(61).

Now the ψ^n are defined as:

$$\phi_{\vec{K}}^{\vec{k}}(\vec{r}, E) = \begin{cases} \frac{1}{\sqrt{V}} e^{i(\vec{k}+\vec{K}).\vec{r}} & \vec{r} \in I \\ \sum_{l,m}(a_{lm}^{\alpha,\vec{k}+\vec{K}} u_l^{\alpha}(r', E) + b_{lm}^{\alpha,\vec{k}+\vec{K}} \dot{u}_l^{\alpha}(r', E)) Y_m^l(\hat{r}') & r' < S_{\alpha} \end{cases}, \quad (16)$$

and the potential is defined as:

$$V(\vec{r}) = \begin{cases} \sum_{lm} V_{lm}(r) Y_{lm}(\hat{r}) & inside\ spheres \\ \sum_{\vec{k}} V_{\vec{k}}\, e^{i\vec{k}.\vec{r}} & outside\ spheres \end{cases}. \quad (17)$$

Chapter Three

Results and Discussion

3.1 Computational method

This research employed the Wien2k package (69) to calculate the structural, electronic, magnetic, and elastic properties, leveraging a Fortran-based (70) software grounded in the FP-LAPW method (69, 70) and the GGA framework (71).

Firstly, we took the lattice parameter values from the results in Granja del toro et al. paper obtained by SIESTA code.

The muffin-tin radii for the elements Fe, Mn, and In in a regular Fe_2MnIn alloy are all identified as 2.35 a.u. In contrast, for the inverse Fe_2MnIn alloy, the muffin-tin radii of Fe, Mn, and In are determined to be 2.37 a.u. each. These values are obtained by the WIEN2k program itself. Where the program gives values for the muffin tin radii that suit the values of the lattice parameters so that we do not have overlap, which leads to giving error in the calculations.

The Au, Mn, and In elements in a conventional Au_2MnIn alloy have muffin-tin radii uniformly set at 2.5 a.u., and this remains true for the inverse Au_2MnIn alloy as well.

The plane wave count, limited by $R_{MT}\times K_{MAX}$, is fixed at 8, with the wave function expansion, labeled L, set to 10. Within the irreducible Brillouin Zone (BZ), 165 k-points are sampled using a (17×17×17) Monkhorst-Pack (MP) grid (72), corresponding to 5000 k-points across the full BZ. This mesh ensures self-consistency for both normal and inverse Fe_2MnIn and Au_2MnIn compounds, and the crystal's total energy converges in self-consistent calculations when it falls below 10^{-5} Ry.

The energy threshold separating core and valence states is established at -9 Ry for the full Heusler alloys Fe_2MnIn and Au_2MnIn.

Elastic analyses establish G_{max} at 14 with L at 8, incorporating 165 k-points in the irreducible Brillouin Zone (BZ) using a 17×17×17 mesh.

The PBE-GGA approach (71) is applied to model the exchange-correlation potential, while the modified Becke-Johnson potential (73) is used to improve the band gap energy in Fe_2MnIn and Au_2MnIn full Heusler alloys.

3.2 Structural properties

This work assesses the structural attributes, including the optimized lattice constant (a), bulk modulus (B), first pressure derivative (B′), and minimum energy (E0), which were computed for normal Fe_2MnIn, normal Au_2MnIn, inverse Fe_2MnIn, and inverse Au_2MnIn.

These results were obtained by applying Murnaghan's equation of state (EOS) to fit the total energy as a function of volume (74).

$$E(V) = E_0 + \frac{VB}{B'}\left\{\left[\frac{\left(\frac{V_0}{V}\right)^{B'}}{B'-1}\right] + 1\right\} - \frac{BV_0}{B'-1} \ , \qquad (18)$$

where $B = -V\frac{dP}{dV}$ and pressure $P = -\frac{dE}{dV}$.

The optimal lattice constant is determined by minimizing the total energy concerning volume, which further allows for the calculation of structural parameters like bulk modulus and the first pressure derivative in cubic Fe_2MnIn and Au_2MnIn compounds, both in their normal and inverse configurations.

Fe2MnIn and Au_2MnIn, as conventional Heusler alloys, are assigned the space group Fm-3m (225), while their inverse counterparts display the distinct F-43m (216) symmetry.

Figure 5 illustrates the crystal structures, while the structural parameters are obtained by fitting the total energy as a function of volume, as depicted in Figure 6, using Murnaghan's equation of state (EOS).

The data in Figure 6 indicate that the stability of crystal structures is higher in ferromagnetic (FM) cases than in non-magnetic (NM) ones, as reflected by the lower energy values in the FM state.

In conclusion, our data are benchmarked against other theoretical predictions and collectively reported in Table 1.

Figure 5

The schematic Representation of the Crystal structure

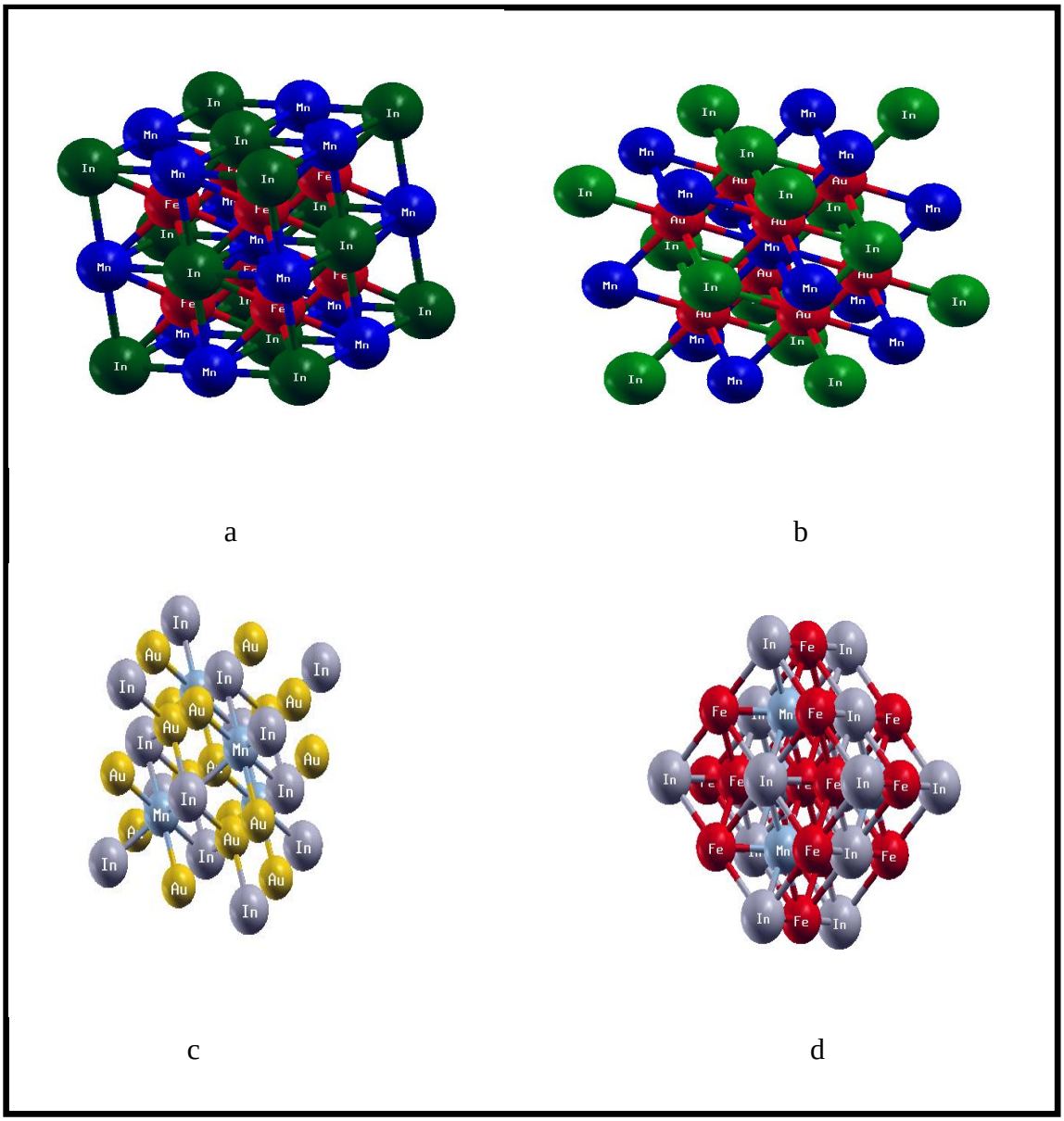

Note: (a) normal Fe_2MnIn (b) normal Au_2MnIn (c) inverse Fe_2MnIn (d) inverse Au_2MnIn compounds.

Figure 6

The variation of total energy with volume

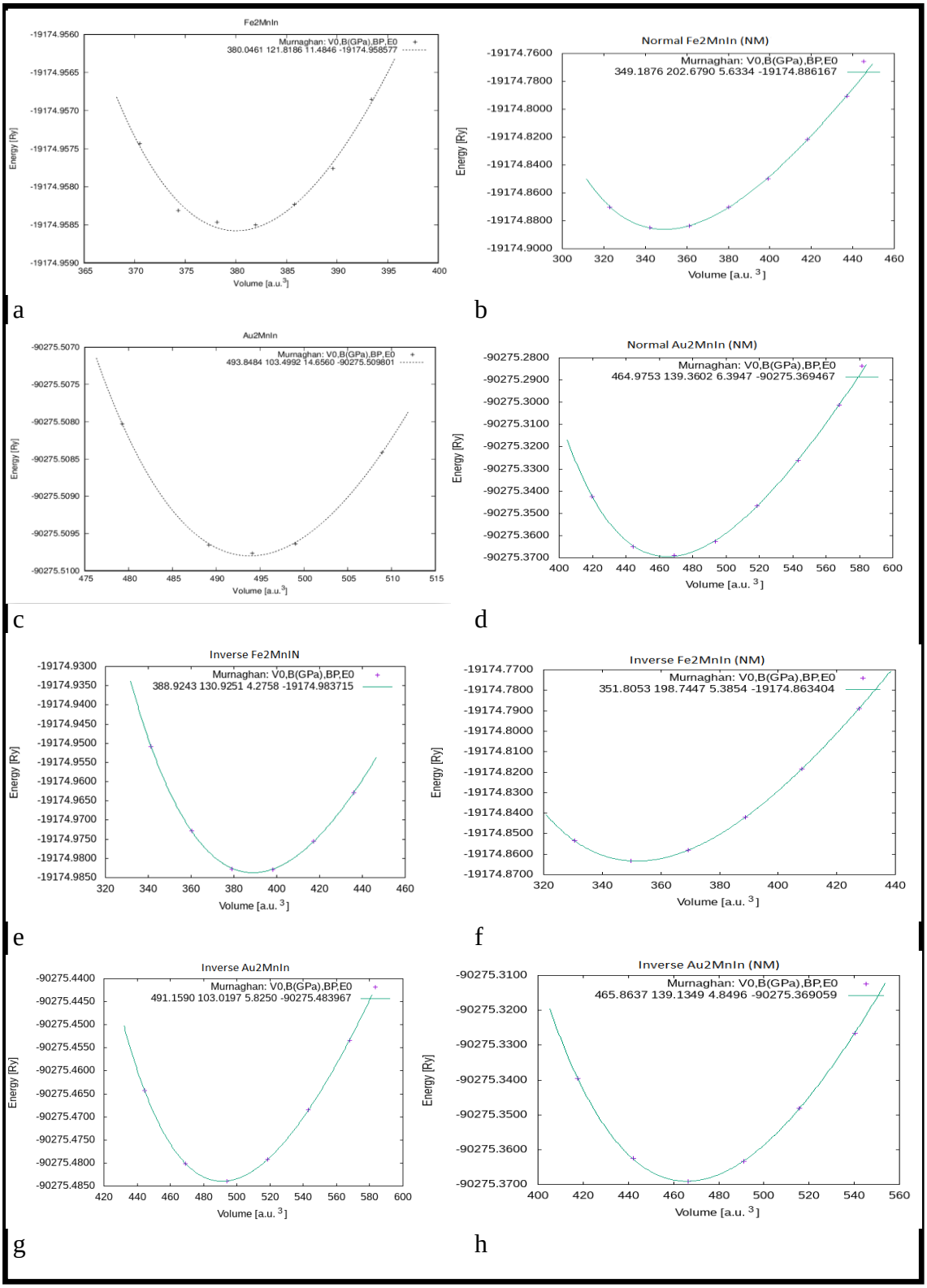

Note: (a) normal Heusler Fe_2MnIn (225) FM (b) normal Heusler Fe_2MnIn (225) NM (c) normal Heusler Au_2MnIn (225) FM (d) normal Heusler Au_2MnIn (225) NM (e) inverse Heusler Fe_2MnIn (216) FM (f) inverse Heusler Fe_2MnIn (216) NM (g) inverse Heusler Au_2MnIn (216) FM (h) inverse Heusler Au_2MnIn (216) NM compounds.

Table 1

Structural and Mechanical Properties of Fe_2MnIn and Au_2MnIn: Lattice Parameters, Bulk Modulus, and Pressure Derivative

Compounds	Source	Lattice constant (Å)	B (GPa)	B' (GPa)
Normal Fe_2MnIn	Present	6.0845	121.7642	12.2077
	SIESTA code (75)	6.197		
Normal Au_2MnIn	Present	6.6397	102.9997	14.7329
	SIESTA code (75)	6.726		
Inverse Fe_2MnIn	Present	6.1308	133.9901	4.7936
	Theoretical			
Inverse Au_2MnIn	Present	6.6277	103.0197	5.8250
	Theoretical			

Optimized lattice parameters, bulk modulus (B), and their first pressure derivatives (B') at zero pressure (0 *GPa*) appear in Table 1, with the noteworthy caveat that the lattice parameters are underestimated when juxtaposed with theoretical data (75).

3.3 Magnetic Properties

The magnetic moments, both total and partial, of Fe_2MnIn and Au_2MnIn full Heusler alloys in their normal and inverse structures, are evaluated within this section. Additionally, the results obtained are subjected to a comparative analysis with other existing theoretical findings (75) and presented in Tables 2 to 5.

Table 2

Magnetic moments, both total and partial, of the standard Fe_2MnIn compound

Compounds	reference	Magnetic moment (μ_B)				
		Fe	Mn	In	Interstitial	MMTOT
Normal Fe_2MnIn	Present	2.38301	2.58673	-0.08092	-0.21206	7.05978
	Theoretical (75)	2.428	3.134	-0.130		7.86

Table 3

Total magnetic moment and its partial contributions in the normal Au_2MnIn compound

Compounds	reference	Magnetic moment (μ_B)				
		Au	Mn	In	Interstitial	MMTOT
Normal Au_2MnIn	Present	0.00984	4.01740	-0.03460	0.05008	4.05256
	Theoretical (75)	0.004	4.324	-0.237		4.09

Table 4

Total magnetic moment and its partial contributions in the normal Fe_2MnIn compound

Compounds	reference	Magnetic moment (μ_B)					
		Fe	Fe	Mn	In	Interstitial	MMTOT
Inverse Fe2MnIn	Present	2.48962	2.46782	3.24004	-0.06636	-0.13125	7.99987
	Theoretical						

Table 5

Total and partial magnetic moment of inverse Au_2MnIn compound.

Compounds	reference	Magnetic moment (μ_B)					
		Au	Au	Mn	In	Interstitial	MMTOT
Inverse Au_2MnIn	Present	0.00355	0.02694	3.88427	-0.04828	0.04588	3.91235
	Theoretical						

The results clearly demonstrate that all compounds display ferromagnetic properties, with the total magnetic moment of normal Au_2MnIn closely matching theoretical expectations, whereas the total magnetic moment of normal Fe_2MnIn is lower than initial

3.4 Electronic properties

Electronic band structures, along with the total and partial densities of states (DOS and PDOS), are assessed for the Au_2MnIn and Fe_2MnIn full Heusler alloys.

3.4.1 Band structure

In this segment, the electronic band structures of the normal and inverse configurations of Fe_2MnIn and Au_2MnIn alloys are examined. Figures 7-10 clearly show that inverse Fe_2MnIn exhibits half-metallic behavior, acting as a metal in one spin direction and as a semiconductor in the other, while the other alloys, including normal Fe_2MnIn, normal Au_2MnIn, and inverse Au_2MnIn, maintain metallic properties in the ferromagnetic phase.

As illustrated in Figure 7, normal Fe_2MnIn, normal Au_2MnIn, inverse Fe_2MnIn, and inverse Au_2MnIn exhibit metallic behavior with zero band gap energy in the spin-up case, as calculated using the PBE-GGA potential.

In the spin-down case depicted in Figure 8, normal Fe_2MnIn, normal Au_2MnIn, and inverse Au_2MnIn exhibit metallic behavior with a zero-energy band gap. In contrast, inverse Fe_2MnIn displays half-metallic behavior with a zero-energy band gap for spin-up and 0.15 eV for spin-down.

In Figure 9, normal Fe_2MnIn, normal Au_2MnIn, inverse Fe_2MnIn, and inverse Au_2MnIn exhibit metallic behavior with zero band gap energy in the majority-spin case, employing the mBJ-GGA potential. Meanwhile, in the spin-down case shown in Figure 10, inverse Fe_2MnIn behaves as a semiconductor with a band gap energy of 0.25 eV, whereas normal Fe_2MnIn, normal Au_2MnIn, and inverse Au_2MnIn exhibit metallic behavior with a zero-energy band gap.

In general, inverse Fe_2MnIn exhibits half-metallic behavior, whereas normal Fe_2MnIn, normal Au_2MnIn, and inverse Au_2MnIn demonstrate metallic behavior. Furthermore, our observations indicate a clear enhancement in the energy band gap when employing the mBJ potential for inverse Fe_2MnIn.

Figure 7

The spin-up band structures using the PBE-GGA approach

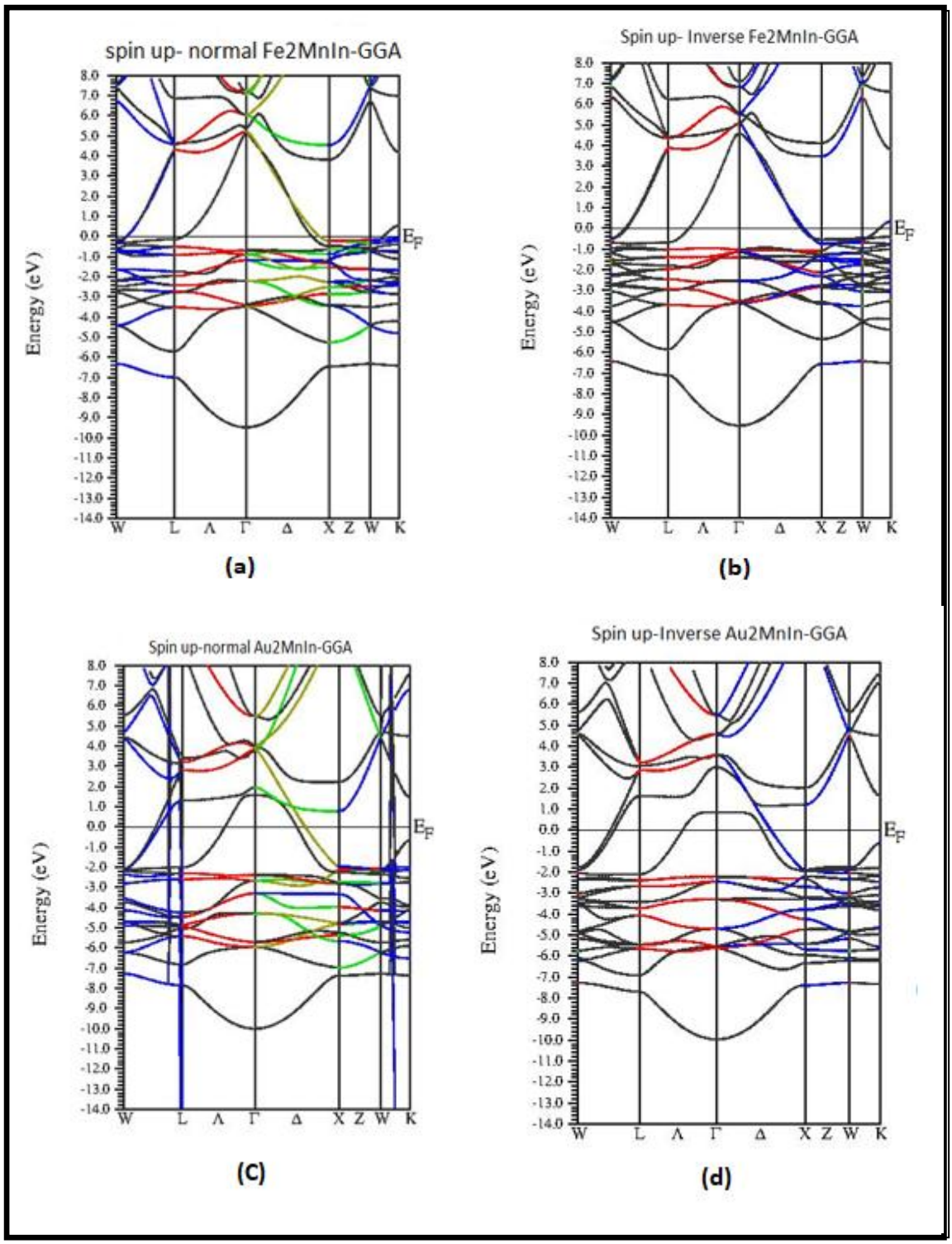

Note: (a) normal Fe_2MnIn, (b) inverse Fe_2MnIn, (c) normal Au_2MnIn, and (d) inverse Au_2MnIn Heusler alloys.

Figure 8

The spin-down band structures using the PBE-GGA approach

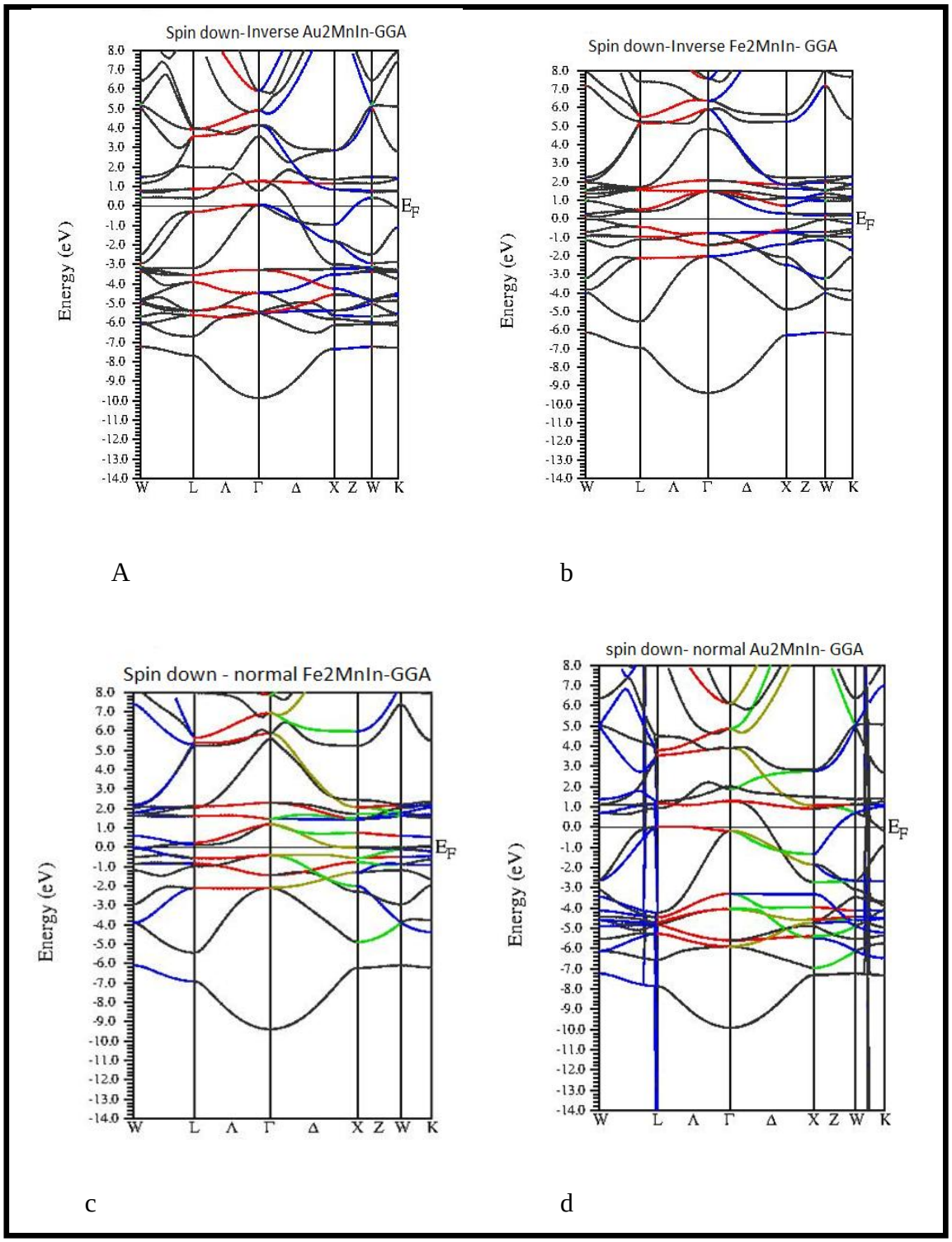

Note: (a) normal Fe_2MnIn, (b) inverse Fe_2MnIn, (c) normal Au_2MnIn, and (d) inverse Au_2MnIn Heusler alloys.

Figure 9

The spin-up band structures using the PBE-GGA approach

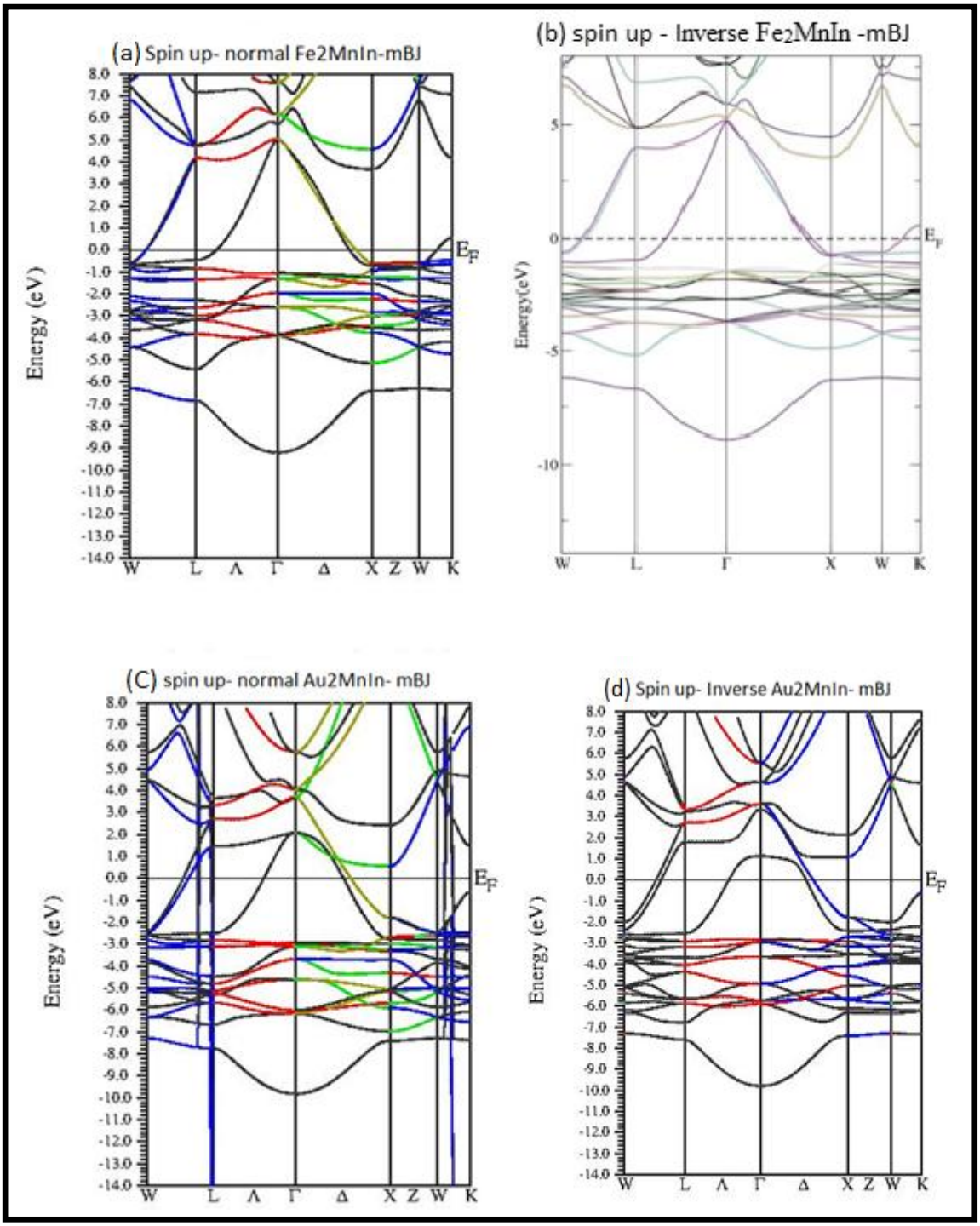

Note: (a) normal Fe_2MnIn, (b) inverse Fe_2MnIn, (c) normal Au_2MnIn, and (d) inverse Au_2MnIn Heusler alloys

Figure 10

The spin-down band structures using the PBE-GGA approach

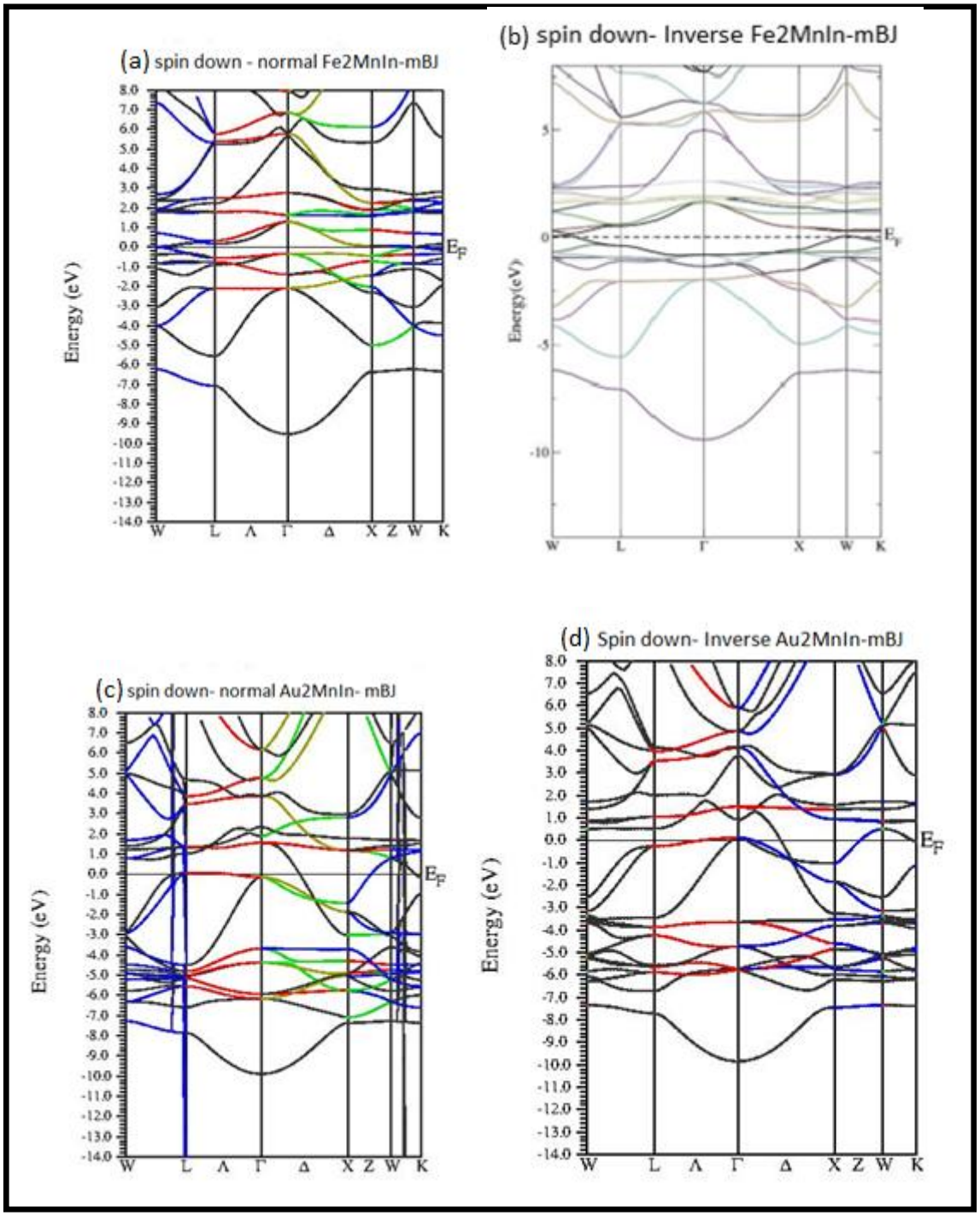

Note: (a) normal Fe_2MnIn, (b) inverse Fe_2MnIn, (c) normal Au_2MnIn, and (d) inverse Au_2MnIn Heusler alloys

Table 6

Band Gap Energies for Fe_2MnIn and Au_2MnIn in Normal and Inverse Structures with PBE and mBJ computational Methods

Full Heusler Alloy		Band-gap type	High-symmetry lines	E_{gap} (PBE-GGA) (*eV*)	E_{gap} (mBJ-GGA) (eV)
Normal Fe_2MnIn					
Inverse Fe_2MnIn	Spin up			Metal	Metal
	Spin down	Direct	W-L	0.15	0.25
Normal Au_2MnIn					
Inverse Au_2MnIn					

3.4.2 Density of States

Figures 11-18 (see Appendix A) display the total and partial density of states (DOS) for both spin-up and spin-down configurations of normal and inverse Fe_2MnIn and Au_2MnIn alloys.

Figure 11 shows the DOS for normal Fe_2MnIn using PBE-GGA. In the spin-up state, the d-states of Fe and Mn predominantly govern the valence and conduction bands, with slight input from the s- and p-states of In, a trend mirrored in the spin-down state, where Fe and Mn d-states lead, and In's s- and p-states contribute minimally.

Figure 12 illustrates the density of states (DOS) for normal Fe_2MnIn, computed with the mBJ-GGA method, showing that the valence and conduction bands in both spin-up and spin-down configurations are predominantly shaped by the d-states of Fe and Mn, with In's s- and p-states contributing minimally.

In Figure 13, the primary contributions to the valence and conduction bands of normal Au_2MnIn in the spin-up case, as observed in the total and partial DOS with PBE-GGA, are predominantly from the d-states of Au and Mn, with a minor contribution from the s- and p-states of In. In the spin-down case, the d-states of Au and Mn continue to dominate, with a smaller contribution from the s- and p-states of In.

Figure 14 shows that for normal Au_2MnIn in the spin-up case, the primary contributions to the valence and conduction bands in the total and partial DOS, calculated with mBJ-GGA, come from the d-states of Au and Mn, with a small contribution from the s- and p-states of In In the spin-down case, this trend continues, with the d-states of Au and Mn remaining dominant, and In's s- and p-states contributing less.

Figure 15 shows that for the spin-up setup of inverse Fe_2MnIn under PBE-GGA, partial and total density of states (DOS) are dominated by d-states of the two Fe and Mn atoms with an extremely small contribution from s- and p-states of In.

Figure 16 reveals that for inverse Fe_2MnIn under the mBJ-GGA approach in the spin-up configuration, the valence and conduction bands of the total and partial DOS are predominantly shaped by the d-states of the two Fe atoms and Mn, with a minor contribution from the s- and p-states of In. In the spin-down structure, this pattern persists, with the d-states of Mn and Fe making important contributions, while In's s- and p-states have a smaller impact.

In Figure 17, the valence and conduction bands for inverse Au_2MnIn, calculated with PBE-GGA in the spin-up case, are predominantly influenced by the d-states of the two Au atoms and the d-state of Mn, with a slight contribution from the s- and p-states of In. For the spin-down scenario, the primary contributions arise from the d-states of the two Au atoms and Mn, while In's s- and p-states play a minor role.

3.5 Elastic Properties

In this computational study, the evaluation was carried out for the bulk modulus (B), shear modulus (S), Young's modulus (Y), Poisson's ratio (ν), anisotropy index (A), and Pugh's ratio (B/S) of the inverse Fe_2MnIn and normal Au_2MnIn compounds. This confirmed their adherence to the standard stability criteria for cubic crystals: $C_{11} > 0$, $C_{11} - C_{12} > 0$, $C_{11} + 2C_{12} > 0$, and $C_{44} > 0$.

The mechanical stability conditions showed that the normal Fe_2MnIn compound and inverse Au_2MnIn exhibit instability, as evidenced by a negative ($C_{11} - C_{12}$) value. In contrast, the normal Au_2MnIn and inverse Fe_2MnIn compounds are mechanically stable. Hence, further investigation into the elastic properties of the normal Fe_2MnIn and inverse Au_2MnIn compounds is not necessary, with C_{11} values systematically

recorded in Table 1.From these conditions, it was observed that the normal Fe_2MnIn compound and the inverse Au_2MnIn are mechanically unstable due to a negative value for (C_{11} - C_{12}), while the normal Au_2MnIn and the inverse Fe_2MnIn are mechanically stable. Therefore, no further study of the elastic properties of normal Fe_2MnIn and inverse Au_2MnIn is required (the C_{11} results are systematically recorded in Table 1).

Table 7

Elastic constants (C_{ii}) of normal and inverse Au_2MnIn and Fe_2MnIn alloys

Compound	C_{11} (GPa)	C_{12} (GPa)	C_{44} (GPa)
Normal Au_2MnIn	103.607	102.28	45.546
Inverse Fe_2MnIn	147.516	125.9796	111.2580
Inverse Au_2MnIn	89.6382	111.4202	206.7976
Normal Fe_2MnIn	80.835	127.955	95.752

We used the Voigt (S_v), Reuss (S_R), and Hill (S_H) approximations to calculate the shear modulus of Au_2MnIn using the following equations (77):

$$S_v = \frac{1}{5}(C_{11} - C_{12} + 3C_{44}). \quad (19)$$

$$S_R = \frac{5C_{44}(C_{11}-C_{12})}{4C_{44}+3(C_{11}-C_{12})}. \quad (20)$$

$$S_H = \frac{S_v+S_R}{2}. \quad (21)$$

Bulk modulus is calculated by the giving formula (77,78):

$$B = \frac{1}{3}(C_{11} + 2C_{12}). \quad (22)$$

The proportion between stress and strain called Young's modulus and giving by the following formula (77):

$$Y = \frac{9BS_v}{S_v+3B}. \quad (23)$$

The Zener anisotropy factor (79) and Poisson's ratio can be expressed through the relationships provided below (77):

$$A = \frac{2C_{44}}{C_{11}-C_{12}}. \quad (24)$$

$$v = \frac{3B-2S_v}{2(3B+S_v)} \ . \quad (25)$$

Hardness in materials can be calculated based on the shear (*S*) and bulk (*B*) moduli (80), whereas Young's modulus is utilized to determine stiffness (81).

Pugh's ratio (B/S) defines the relationship between the bulk and shear moduli. Materials with a (B/S) ratio greater than 1.75 and a Voigt Poisson's ratio (ν) above 0.26 demonstrate ductile properties, whereas those with a (B/S) ratio of 1.75 or lower and a Voigt Poisson's ratio (ν) below 0.26 exhibit brittle characteristics (77, 78).

Material anisotropy is quantified by the anisotropic index (A) (79, 82); a value of 1 denotes isotropy, whereas divergence from 1 suggests elastic anisotropy (82, 83).

Finally, the bonding nature is inferred from the ν value. Compounds with a ν below 0.25 typically show covalent bonding, while those with a ν between 0.25 and 0.5 demonstrate ionic bonding (77).

Table 8

The bulk modulus (B), shear modulus (S), Young's modulus (Y), Poisson's ratio (v), anisotropic index (A), and Pugh's ratio (B/S) of normal Au_2MnIn and inverse Fe_2MnIn alloys

Compound	Bulk Modulus B (*GPa*)	Shear Modulus S (*GPa*)	B/S ratio	Young's Modulus Y (*GPa*)	Poisson's Ratio *v*	Anisotropy Index A
Normal Au_2MnIn	102.722	27.593	3.7228	75.976	0.377	68.645
Inverse Fe_2MnIn	133.1584	71.062	1.873	180.9899	0.273	10.332

An examination of Table 8 reveals that both normal Au_2MnIn and inverse Fe_2MnIn compounds exhibit ductile behavior. Furthermore, these compounds display elastic anisotropy and are characterized by ionic bonding.

Additionally, by comparing the bulk modulus values of normal Au_2MnIn and inverse Fe_2MnIn, which were obtained by optimizing the lattice parameters (102.9997 GPa and 133.9901 GPa, respectively), with those derived from the elastic constants (102.722 GPa and 133.1584 GPa, respectively), we found that the values are in good agreement with each other.

Chapter Four

Conclusion

This study provides a theoretical examination of structural, electronic, magnetic, and elastic properties of Fe_2MnIn and Au_2MnIn Full Heusler compounds using Full Potential Linearized Augmented Plane Wave method in combination with Density Functional Theory.

The lattice parameters of 6.0845 Å and 6.6397 Å were optimized for normal Fe_2MnIn and Au_2MnIn, respectively, while the inverse configurations give values of 6.1308 Å and 6.6277 Å, respectively.

Furthermore, both normal and inverse forms of Fe_2MnIn and Au_2MnIn exhibit ferromagnetic character. Magnetic moments in these compounds have been computed to be 7.05978 μ_B for normal Fe_2MnIn, 4.05256 μ_B for normal Au_2MnIn, 7.99987 μ_B for inverse Fe_2MnIn, and 3.91235 μ_B for inverse Au.The electronic characteristics reveal that the inverse Fe_2MnIn alloy demonstrates half-metallic properties, with a band gap of 0.25 eV, calculated using the mBJ-GGA approach. In contrast, normal Fe_2MnIn, normal Au_2MnIn, and inverse Au_2MnIn exhibit metallic behavior with zero band gap energy.

In conclusion, the examination of elastic properties reveals that normal Fe_2MnIn and inverse Au_2MnIn compounds display mechanical instability, while normal Au_2MnIn and inverse Fe_2MnIn compounds show mechanical stability. Pugh's ratio findings indicate that the normal Au_2MnIn and inverse Fe_2MnIn compounds exhibit ductile behavior. Additionally, Poisson's ratio measurements indicate that both normal Au_2MnIn and inverse Fe_2MnIn alloys exhibit ionic bonding and display elastic anisotropy.

List of Abbreviations

Abbreviation	Meaning
FP-LAPW	Full Potential Linearized Augmented Planewave
FCC	Face Centered Cubic.
DFT	The method of Density Functional Theory.
GGA	The Generalized Gradient Approximation technique.
mBJ	The Modified Becke-Johnson approach.
Eos	Equation Of State.
DOS	Density Of State.
HH	Half Heusler.
DMS	Dilute Magnetic Semiconductors.
GMR	Giant Magneto Resistance.
MRAM	A type of Magnetic Random-Access Memory.
DRAM	Known as Dynamic Random-Access Memory.
SRAM	Referring to Static Random-Access Memory.
MSM	Magnetic Shape Memory.
LDA	Local Density Approximation.
LAPW	Linearized Augmented Planewave
BZ	Brillouin zone
MP	Monkhorst Pack.
IBZ	irreducible Brillouin zone.
NM	Nonmagnetic.
FM	Ferromagnetic.
PDOS	Partial Density of State.
TDOS	Total Density of State.

References

1. Guermit Y, Drief M, Benkhettou N, Lantri T, Rached D. Electronic and elastic properties of Ba2HgSn and Ca2HgSn Rattling Heusler. J Phys Conf Ser. 2018;1081(1):7–13.

2. El Krimi Y, Masrour R, Jabar A. Electronic, magnetic, elastic, thermal and thermoelectric proprieties of Co2MnZ (Z=Al, Ge, Sn). J Mol Graph Model [Internet]. 2022;114(March):108165. Available from: https://doi.org/10.1016/j.jmgm.2022.108165

3. Casper F, Graf T, Chadov S, Balke B, Felser C. Half-Heusler compounds: novel materials for energy and spintronic applications. Semicond Sci Technol. 2012 Jun 13;27(6):063001.

4. Graf T, Felser C, Parkin SSP. Simple rules for the understanding of Heusler compounds. Prog Solid State Chem. 2011 May;39(1):1–50.

5. Wollmann L, Nayak AK, Parkin SSP, Felser C. Heusler 4.0: Tunable Materials. 2016 Dec 18; Available from: http://arxiv.org/abs/1612.05947

6. Elphick K, Frost W, Samiepour M, Kubota T, Takanashi K, Sukegawa H, et al. Heusler alloys for spintronic devices: review on recent development and future perspectives. Vol. 22, Science and Technology of Advanced Materials. Taylor and Francis Ltd.; 2021. p. 235–71.

7. Webster PJ. Heusler alloys. Contemp Phys. 1969 Nov;10(6):559–77.

8. Albert James Bradley, J. W. Rodgers. The crystal structure of the heusler alloys. Proc R Soc London Ser A, Contain Pap a Math Phys Character. 1934 Mar 29;144(852):340–59.

9. Nakata J, Terada Y, Takizawa S, Ohkubo K, Mohri T, Suzuki T. Thermal Conductivity in <I>X</I>₂<I>YZ</I> Heusler Type Intermetallic Compounds. Mater Trans JIM. 1996;37(3):442–7.

10. Mohanta SK, Tao Y, Yan X, Qin G, Chandragiri V, Li X, et al. First principles electronic structure and magnetic properties of inverse Heusler alloys X2YZ(X=Cr; Y=Co, Ni; Z=Al, Ga, In, Si, Ge, Sn, Sb). J Magn Magn Mater. 2017;430(November 2016):65–9.

11. Fomina KA, Marchenkov V V., Shreder EI, Weber HW. Electrical and optical properties of X2YZ (X = Co, Fe; Y = Cr, Mn, Ti; Z = Ga, Al, Si) Heusler alloys. Solid State Phenom. 2011;168–169(December 2010):545–8.

12. Ma J, Hegde VI, Munira K, Xie Y, Keshavarz S, Mildebrath DT, et al. Computational investigation of half-Heusler compounds for spintronics applications. Phys Rev B. 2017 Jan 11;95(2):024411.

13. Galanakis I, Mavropoulos P, Dederichs PH. Electronic structure and Slater–Pauling behaviour in half-metallic Heusler alloys calculated from first principles. J Phys D Appl Phys. 2006 Mar 7;39(5):765–75.

14. Benkabou M, Rached H, Abdellaoui A, Rached D, Khenata R, Elahmar MH, et al. Electronic structure and magnetic properties of quaternary Heusler alloys CoRhMnZ (Z = Al, Ga, Ge and Si) via first-principle calculations. J Alloys Compd. 2015 Oct;647:276–86.

15. Abu Baker DN, Abu-Jafar MS, Mousa AA, Jaradat RT, Ilaiwi KF, Khenata R. Structural, magnetic, electronic and elastic properties of half-metallic ferromagnetism full-Heusler alloys: Normal-Co2TiSn and inverse- Zr2RhGa using FP-LAPW method. Mater Chem Phys [Internet]. 2020;240(August 2019):122122. Available from: https://doi.org/10.1016/j.matchemphys.2019.122122

16. Sokolovskiy V, Zagrebin M, Buchelnikov VD. First-principles study of Ni-Co-Mn-Sn alloys with regular and inverse Heusler structure. J Magn Magn Mater. 2019 Apr;476:546–50.

17. Chatterjee S, Chatterjee S, Giri S, Majumdar S. Transport properties of Heusler compounds and alloys. J Phys Condens Matter. 2022 Jan 5;34(1):013001.

18. Ayuela A, Enkovaara J, Ullakko K, Nieminen RM. Structural properties of magnetic Heusler alloys. J Phys Condens Matter. 1999 Mar 1;11(8):2017–26.

19. Palmstrøm CJ. Heusler compounds and spintronics. Prog Cryst Growth Charact Mater. 2016 Jun;62(2):371–97.

20. Kahal L, Ferhat M. Theoretical study of the structural stability, electronic, and magnetic properties of MBi (M=V, Cr, and Mn) compounds. J Appl Phys. 2010 Feb 15;107(4).

21. Rai DP, Shankar A, Sandeep, Ghimire MP, Thapa RK. A comparative study of a Heusler alloy Co 2FeGe using LSDA and LSDA+U. Phys B Condens Matter [Internet]. 2012;407(18):3689–93. Available from: http://dx.doi.org/10.1016/j.physb.2012.04.055

22. Wu Y, Wu B, Wei Z, Zhou Z, Zhao C, Xiong Y, et al. Structural, half-metallic and elastic properties of the half-Heusler compounds NiMnM (M = Sb, As and Si) and IrMnAs from first-principles calculations. Intermetallics. 2014 Oct;53:26–33.

23. Amudhavalli A, Rajeswarapalanichamy R, Iyakutti K. Structural, electronic, mechanical and magnetic properties of Mn based ferromagnetic half Heusler alloys: A first principles study. J Alloys Compd [Internet]. 2017;708:1216–33. Available from: http://dx.doi.org/10.1016/j.jallcom.2017.03.092

24. Gupta DC, Ghosh S. First-principal study of full Heusler alloys Co2VZ (Z = As, In). J Magn Magn Mater [Internet]. 2017;435:107–16. Available from: http://dx.doi.org/10.1016/j.jmmm.2017.03.067

25. Ahmed R, Masuri NS, Ul Haq B, Shaari A, AlFaifi S, Butt FK, et al. Investigations of electronic and thermoelectric properties of half-Heusler alloys XMgN (X = Li, Na, K) by first-principles calculations. Mater Des. 2017;136:196–203.

26. Zhang L, Wang X, Cheng Z. Electronic, magnetic, mechanical, half-metallic and highly dispersive zero-gap half-metallic properties of rare-earth-element-based quaternary Heusler compounds. J Alloys Compd. 2017 Sep;718:63–74.

27. Shawahni AM, Abu-Jafar MS, Jaradat RT, Ouahrani T, Khenata R, Mousa AA, et al. Structural, Elastic, Electronic and Optical Properties of SrTMO3 (TM = Rh, Zr) Compounds: Insights from FP-LAPW Study. Materials (Basel). 2018 Oct 22;11(10):2057.

28. Jain R, Lakshmi N, Jain VK, Jain V, Chandra AR, Venugopalan K. Electronic structure, magnetic and optical properties of Co2TiZ (Z = B, Al, Ga, In) Heusler alloys. J Magn Magn Mater. 2018 Feb;448:278–86.

29. Fadila B, Ameri M, Bensaid D, Noureddine M, Ameri I, Mesbah S, et al. Structural, magnetic, electronic and mechanical properties of full-Heusler alloys Co2YAl (Y = Fe, Ti): First principles calculations with different exchange-correlation potentials. J Magn Magn Mater. 2018 Feb;448:208–20.

30. Mehmood N, Ahmad R. Structural, Electronic, Magnetic, and Optical Properties of Half-Heusler Alloys RuMnZ (Z = P, As): a First-Principle Study. J Supercond Nov Magn. 2018 Jan 22;31(1):233–9.

31. Huang HM, Zhang CK, He ZD, Zhang J, Yang JT, Luo SJ. Electronic and mechanical properties of half-metallic half-Heusler compounds CoCr *Z* (*Z* = S, Se, and Te). Chinese Phys B. 2018 Jan;27(1):017103.

32. Mokhtari, Dahmane, Benabdellah, Zekri, Benalia, Zekri. Theoretical study of the structural stability, electronic and magnetic properties of XVSb (X = Fe, Ni, and Co) half-Heusler compounds. Condens Matter Phys. 2018 Dec;21(4):43705.

33. El Krimi Y, Masrour R, Jabar A. Structural, electronic and magnetic properties of full-Heusler alloy Co2CrAl. Inorg Chem Commun [Internet]. 2020 Nov;121:108207. Available from: https://linkinghub.elsevier.com/retrieve/pii/S1387700320307978

34. Wakeel M, Murtaza G, Ullah H, Khan S, Laref A, Ameer Z, et al. Structural, electronic, and magnetic properties of palladium based full Heusler compounds: DFT study. Phys B Condens Matter. 2021 May;608:412716.

35. Yahya SJ, Abu-Jafar MS, Al Azar S, Mousa AA, Khenata R, Abu-Baker D, et al. The Structural, Electronic, Magnetic and Elastic Properties of Full-Heusler Co2CrAl and Cr2MnSb: An Ab Initio Study. Crystals. 2022 Nov 6;12(11):1580.

36. Saim A, Belkharroubi F, Boufadi FZ, Ameri I, Blaha LF, Tebboune A, et al. Investigation of the Structural, Elastic, Electronic, and Optical Properties of Half-

Heusler CaMgZ (Z = C, Si, Ge, Sn, Pb) Compounds. J Electron Mater. 2022 Jul 10;51(7):4014–28.

37. Jaradat RT, Abu-Jafar MS, Farout M, Azar SM, Khenata R, Mousa AA. Structural, electronic, magnetic, and optical investigations of sodium chalcogenides: First-principles calculations. AIP Adv. 2023 Jan 1;13(1).

38. Al-Masri KM, Abu-Jafar MS, Farout M, Dahliah D, Mousa AA, Azar SM, et al. Structural, Elastic, Electronic, and Magnetic Properties of Full-Heusler Alloys Sc2TiAl and Sc2TiSi Using the FP-LAPW Method. Magnetochemistry [Internet]. 2023 Apr 16;9(4):108. Available from: https://www.mdpi.com/2312-7481/9/4/108

39. AlShaikh Mohammad NF, Abu-Jafar MS, Asad JH, Bouhemadou A, Mousa AA, Khenata R, et al. First-principles calculations of structural, elastic, electronic, magnetic, optical, thermoelectric, and dynamic properties of CoCrTe half-Heusler compound. Opt Quantum Electron [Internet]. 2024 May 9;56(6):1049. Available from: https://link.springer.com/10.1007/s11082-024-07002-5

40. AlShaikh Mohammad NF, Abu-Jafar MS, Asad JH, Bouhemadou A, Mousa AA, Khenata R, et al. Investigating of structural, electronic, magnetic, dynamic, and thermoelectric properties of CoCrSe half-Heusler compound using FP-LAPW method. Eur Phys J B [Internet]. 2024 May 8;97(5):56. Available from: https://link.springer.com/10.1140/epjb/s10051-024-00700-9

41. AlShaikh Mohammad NF, Abu-Jafar MS, Asad JH, Farout M, Bouhemadou A, Mousa AA, et al. FP-LAPW study of structural, magnetic, electronic, elastic, and thermoelectric properties of CoCrS Half-Heusler compound. AIP Adv [Internet]. 2024 Apr 1;14(4). Available from: https://pubs.aip.org/adv/article/14/4/045207/3280735/FP-LAPW-study-of-structural-magnetic-electronic

42. Mackay AL. Stereological characteristics of atomic arrangements in crystals. J Microsc. 1972 Apr 2;95(2):217–27.

43. Abdullah D, Gupta DC. Structural, mechanical and dynamical stabilities of K2NaMCl6 (M: Cr, Fe) halide perovskites along with electronic and thermal properties. J Magn Magn Mater. 2023 Mar;569:170474.

44. Connell JH, Sousa WP. On the Evidence Needed to Judge Ecological Stability or Persistence. Am Nat. 1983 Jun;121(6):789–824.

45. Bartel CJ. Review of computational approaches to predict the thermodynamic stability of inorganic solids. J Mater Sci. 2022 Jun 1;57(23):10475–98.

46. Thomas H. Courtney. Mechanical Behavior of Materials: Second Edition. second. Waveland Press; 2005.

47. Born M, Huang K. Dynamical theory of crystal lattices. Oxford university press; 1996.

48. Cullity BD, Graham CD. INTRODUCTION TO MAGNETIC MATERIALS Second Edition.

49. Ishida S, Ishida J, Asano S, Yamashita J. Band Calculation of Cu $_2$ MnAl. J Phys Soc Japan. 1978 Oct;45(4):1239–43.

50. Hummel RE. Electronic Properties of Materials Third Edition With 252 Illustrations.

51. Sankar Das Sarma. Spintronics: A new class of device based on the quantum of electron spin, rather than on charge, may yield the next generation of microelectronics. 2001 Nov;89.

52. Hirohata A, Yamada K, Nakatani Y, Prejbeanu L, Diény B, Pirro P, et al. Review on spintronics: Principles and device applications. Vol. 509, Journal of Magnetism and Magnetic Materials. Elsevier B.V.; 2020.

53. Ohno H, Stiles MD, Dieny B. Scanning the Issue. Proc IEEE. 2016 Oct;104(10):1782–6.

54. Wilson SA, Jourdain RPJ, Zhang Q, Dorey RA, Bowen CR, Willander M, et al. New materials for micro-scale sensors and actuators. An engineering review. Vol. 56, Materials Science and Engineering R: Reports. 2007. p. 1–129.

55. Ullakko K. Magnetically Controlled Shape Memory Alloys: A New Class of Actuator Materials. Vol. 5, JMEPEG. 1996.

56. Schiepp T. A Simulation Method for Design and Development of Magnetic Shape Memory Actuators. 2015.

57. Karaman I, Basaran B, Karaca HE, Karsilayan AI, Chumlyakov YI. Energy harvesting using martensite variant reorientation mechanism in a NiMnGa magnetic shape memory alloy. Appl Phys Lett. 2007;90(17).

58. Hasan MZ, Kane CL. Topological Insulators. 2010 Feb 20; Available from: http://arxiv.org/abs/1002.3895

59. Zhu Z, Cheng Y, Schwingenschlögl U. Band inversion mechanism in topological insulators: A guideline for materials design. Phys Rev B - Condens Matter Mater Phys. 2012 Jun 1;85(23).

60. Qi XL, Zhang SC. Topological insulators and superconductors. 2010 Aug 11; Available from: http://arxiv.org/abs/1008.2026

61. Cottenier S. Density Functional Theory and the Family of (L)APW-methods: a step-by-step introduction. Computer Physics Reports. 2013. 1–9 p.

62. Dixon DA. Density functional theory. Encycl Earth Sci Ser. 2016;1–7.

63. Schwarz K, Blaha P. Solid state calculations using WIEN2k. Comput Mater Sci. 2003;28(2):259–73.

64. Schwarz K. DFT calculations of solids with LAPW and WIEN2k. J Solid State Chem. 2003;176(2):319–28.

65. Perdew JP, Ernzerhof M, Burke K. Origins and Chemical Consequences. 1998;108(4):1522–31.

66. Zhang Y, Sun J, Perdew JP, Wu X. Comparative first-principles studies of prototypical ferroelectric materials by LDA, GGA, and SCAN meta-GGA. Phys Rev B. 2017;96(3).

67. Tran F, Laskowski R, Blaha P, Schwarz K. Performance on molecules, surfaces, and solids of the Wu-Cohen GGA exchange-correlation energy functional. Phys Rev B - Condens Matter Mater Phys. 2007;75(11):1–14.

68. Koller D, Tran F, Blaha P. Merits and limits of the modified Becke-Johnson exchange potential. Phys Rev B - Condens Matter Mater Phys. 2011;83(19):1–10.

69. Blaha P, Schwarz K, Tran F, Laskowski R, Madsen GKH, Marks LD. WIEN2k: An APW+lo program for calculating the properties of solids. J Chem Phys [Internet]. 2020 Feb 21;152(7). Available from: https://pubs.aip.org/jcp/article/152/7/074101/485553/WIEN2k-An-APW-lo-program-for-calculating-the

70. Blaha P, Schwarz K, Madsen GKH, Kvasnicka D, Luitz J, Schwarz K. An augmented plane wave plus local orbitals program for calculating crystal properties: Wien2K User's Guide. Techn Univ Wien. 2008;28(January):28.

71. Perdew JP, Burke K, Ernzerhof M. Generalized Gradient Approximation Made Simple. Phys Rev Lett. 1996 Oct 28;77(18):3865–8.

72. Monkhorst HJ, Pack JD. Special points for Brillouin-zone integrations. Phys Rev B [Internet]. 1976 Jun 15;13(12):5188–92. Available from: https://link.aps.org/doi/10.1103/PhysRevB.13.5188

73. Becke AD, Johnson ER. A simple effective potential for exchange. J Chem Phys [Internet]. 2006 Jun 14;124(22):221101. Available from: https://pubs.aip.org/aip/jcp/article/920551

74. Tyuterev VG, Vast N. Murnaghan's equation of state for the electronic ground state energy. Comput Mater Sci. 2006;38(2):350–3.

75. Aguilera-Granja F, Aguilera-del-Toro RH, Morán-López JL. A first principles systematic study of the structural, electronic, and magnetic properties of Heusler X 2 MnZ with X = Fe, Co, Ni, Cu, Ru, Rh, Pd, Ag, Pt, Au and Z = Al, Si, Ga, Ge, In and Sn. Mater Res Express [Internet]. 2019 Sep 11;6(10):106118. Available from: https://iopscience.iop.org/article/10.1088/2053-1591/ab243c

76. Hashemifar SJ, Kratzer P, Scheffler M. Preserving the half-metallicity at the heusler alloy Co 2MnSi(001) surface: A density functional theory study. Phys Rev Lett. 2005;94(9):1–4.

77. Gupta Y, Sinha MM, Verma SS. Exploring the structural, elastic, lattice dynamical stability and thermoelectric properties of semiconducting novel quaternary Heusler alloy LiScPdPb. J Solid State Chem [Internet]. 2021;304(September):122601. Available from: https://doi.org/10.1016/j.jssc.2021.122601

78. Huang ZW, Zhao YH, Hou H, Han PD. Electronic structural, elastic properties and thermodynamics of Mg 17Al 12, Mg 2Si and Al 2Y phases from first-principles calculations. Phys B Condens Matter [Internet]. 2012;407(7):1075–81. Available from: http://dx.doi.org/10.1016/j.physb.2011.12.132

79. Kube CM. Elastic anisotropy of crystals. AIP Adv [Internet]. 2016 Sep 1;6(9). Available from: https://pubs.aip.org/adv/article/6/9/095209/873497/Elastic-anisotropy-of-crystals

80. Teter DM. Computational alchemy: the search for new superhard materials. MRS Bull. 1998;23(1):22–7.

81. Bonora N, Ruggiero A, Gentile D, De Meo S. Practical applicability and limitations of the elastic modulus degradation technique for damage measurements in ductile metals. Strain. 2011;47(3):241–54.

82. Lethbridge ZAD, Walton RI, Marmier ASH, Smith CW, Evans KE. Elastic anisotropy and extreme Poisson's ratios in single crystals. Acta Mater [Internet]. 2010;58(19):6444–51. Available from: http://dx.doi.org/10.1016/j.actamat.2010.08.006

83. Ravindran P, Fast L, Korzhavyi PA, Johansson B, Wills J, Eriksson O. Density functional theory for calculation of elastic properties of orthorhombic crystals: Application to TiSi2. J Appl Phys. 1998 Nov 1;84(9):4891–904.

Appendices

Appendix A

List of DOS plots

Figure 11

Total and partial density of states of normal Fe_2MnIn in spin up and spin down cases using PBE-GGA

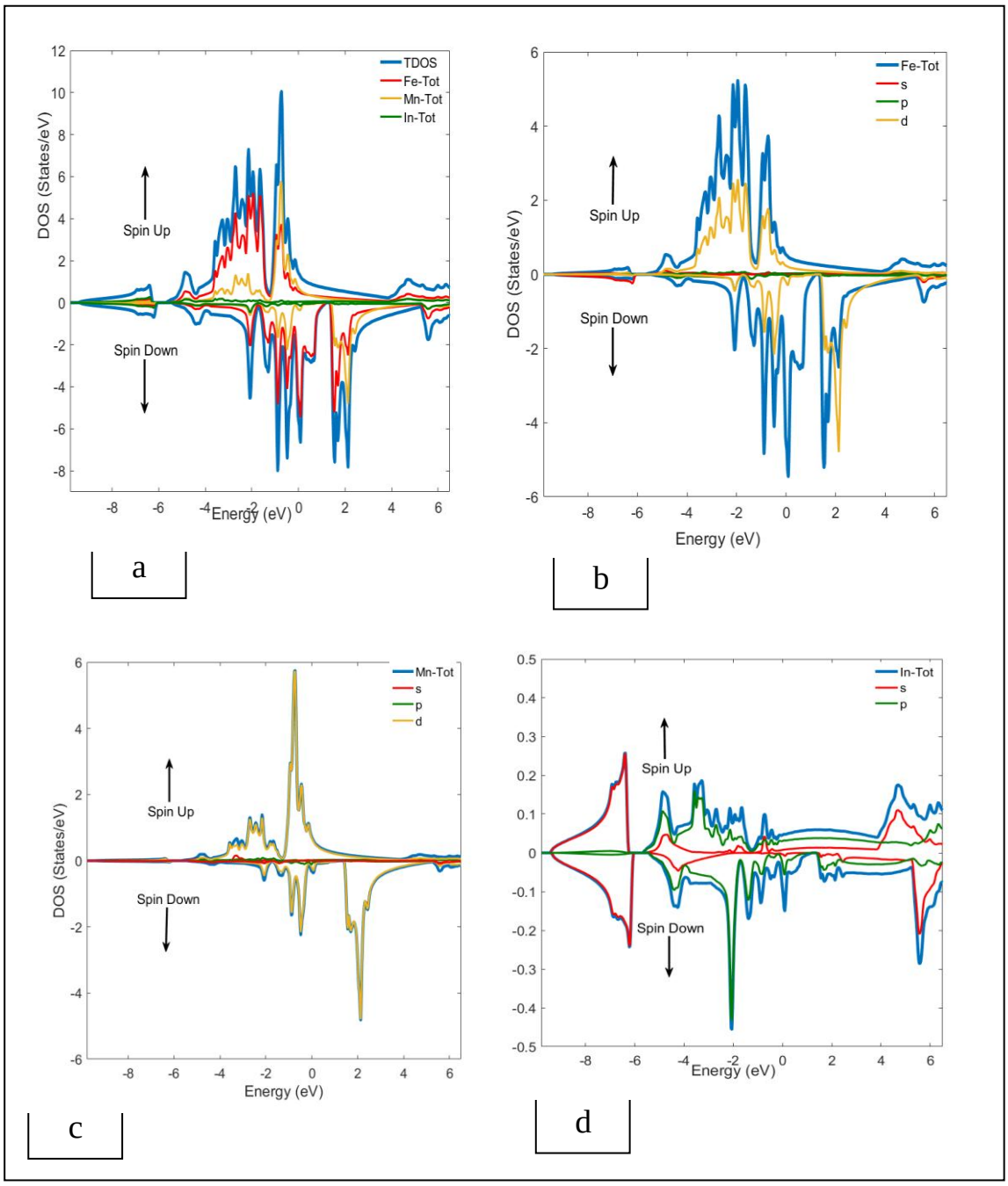

Note: (a) Total density of states (b) Partial density of state of Fe atom(c)Mn atom (d)In atom.

Figure 12

Total and partial density of states of normal Fe_2MnIn in spin up and spin down cases using mBJ-GGA

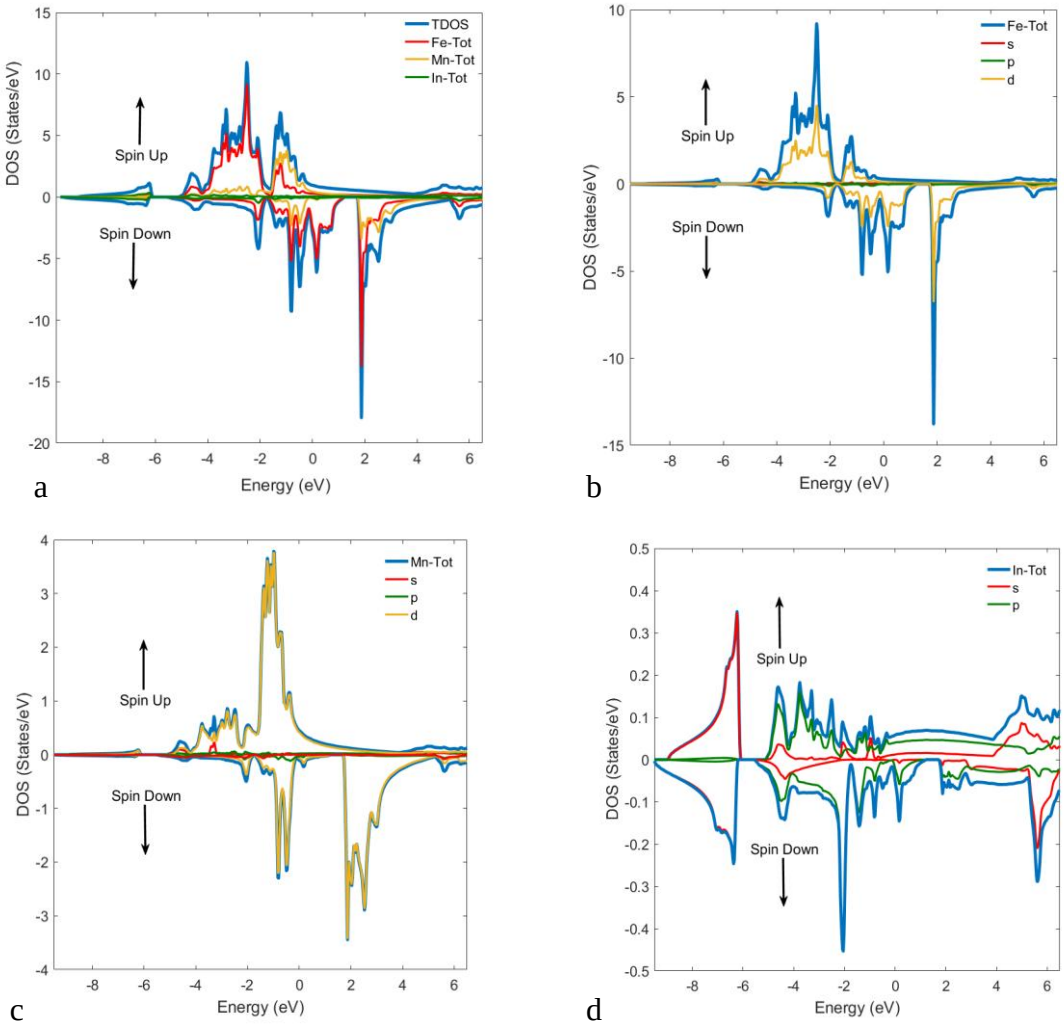

Note: (a) Total density of states (b) partial density of states of Fe atom (c)Mn atom(d)In atom.

Figure 13

Total and partial density of states of normal Au_2MnIn in spin up and spin down cases PBE-GGA

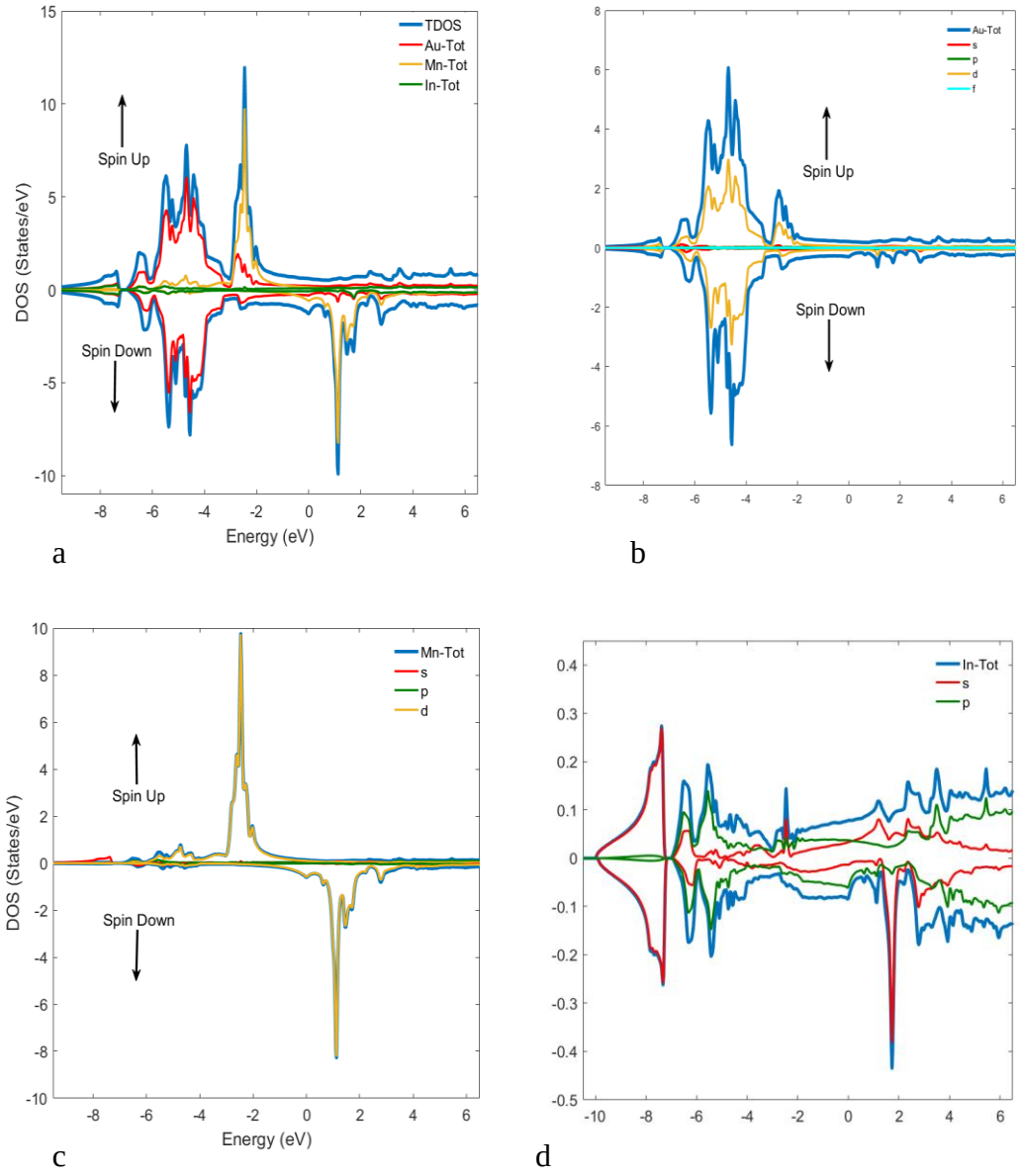

Note: (a) Total density of states (b) partial density of states of Au atom(c)Mn atom(d)In atom.

Figure 14

Total and partial density of states of normal Au_2MnIn in spin up and spin down cases mBJ-GGA

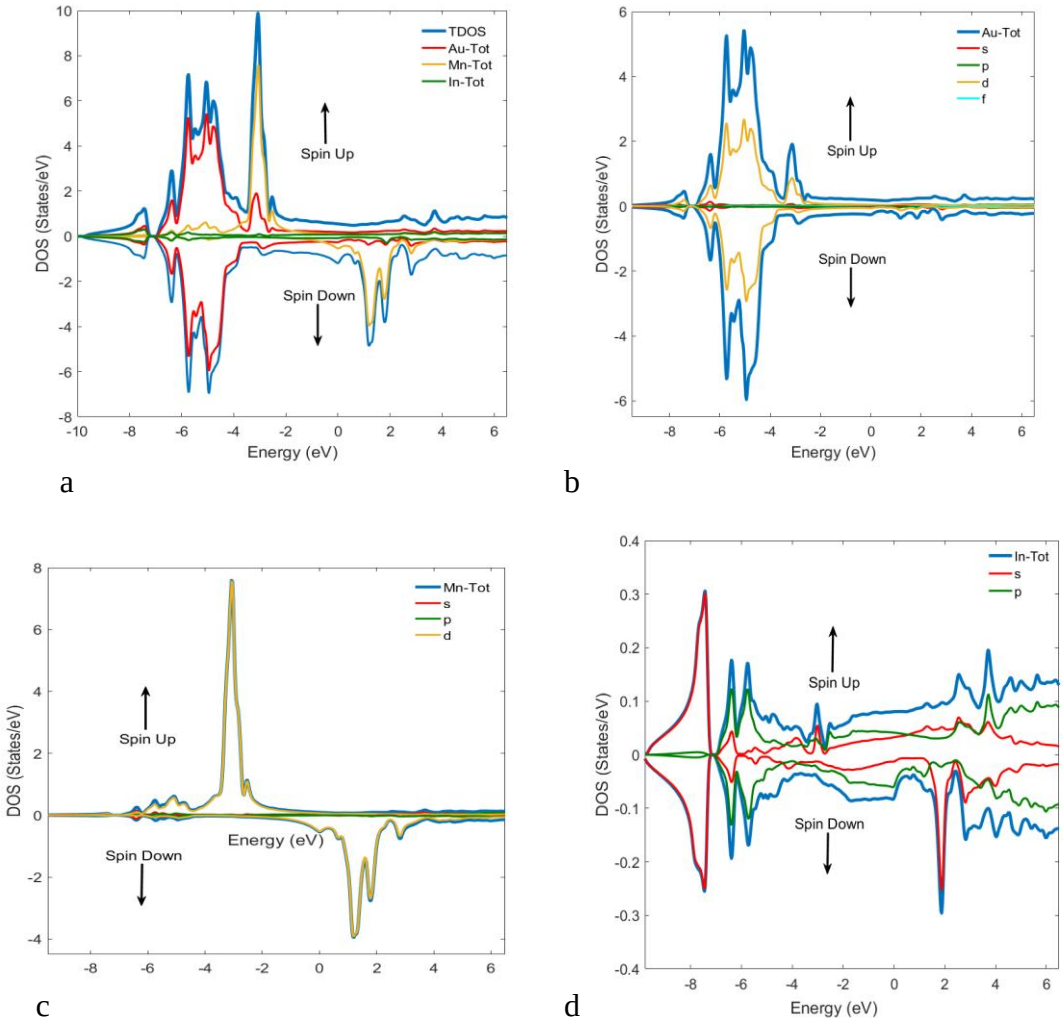

Note: (a) Total density of states (b) partial density of states of Au atom(c)Mn atom(d)In atom.

Figure 15

Total and partial density of states of inverse Au_2MnIn in spin up and spin down cases PBE-GGA

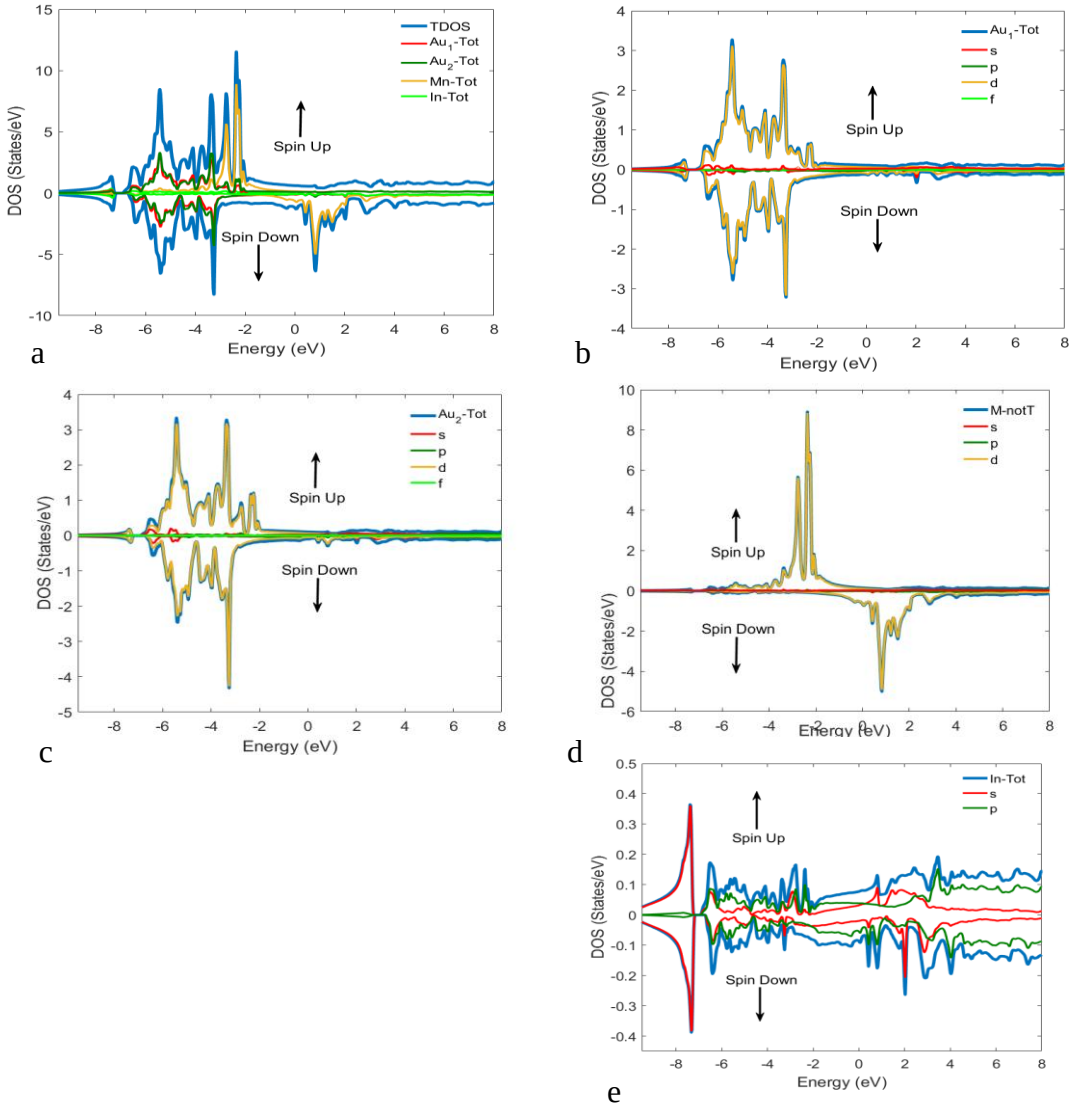

Note: (a) Total density of states (b) partial density of states of Au1 atom(c)Au2 atom (d)Mn atom (e)In atom.

Figure 16

Total and partial density of states of inverse Au_2MnIn in spin up and spin down cases mBJ-GGA

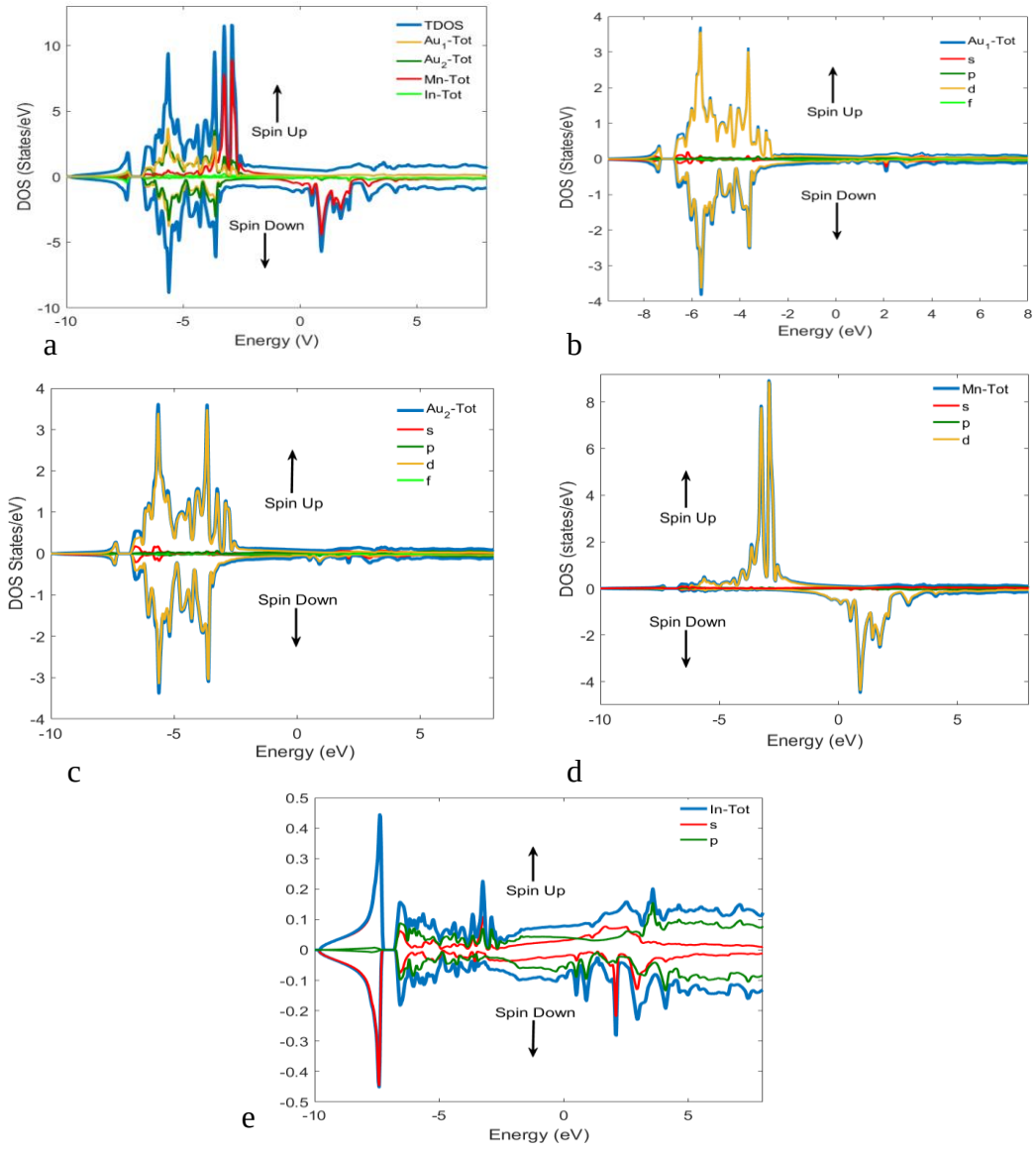

Note: (a) Total density of states (b) partial density of states of Au1 atom(c)Au2 atom (d)Mn atom (e)In atom.

Figure 17

Total and partial density of states of inverse Fe_2MnIn in spin up and spin down cases using PBE-GGA

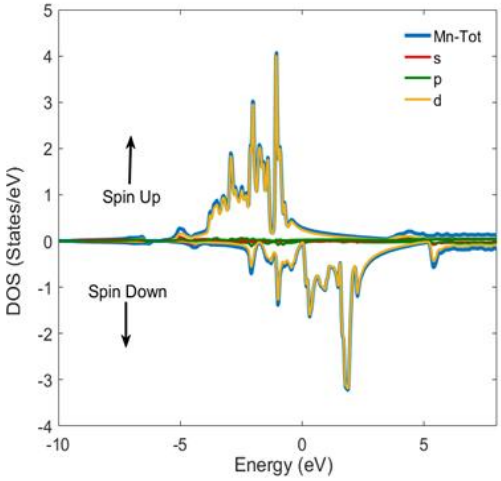

a

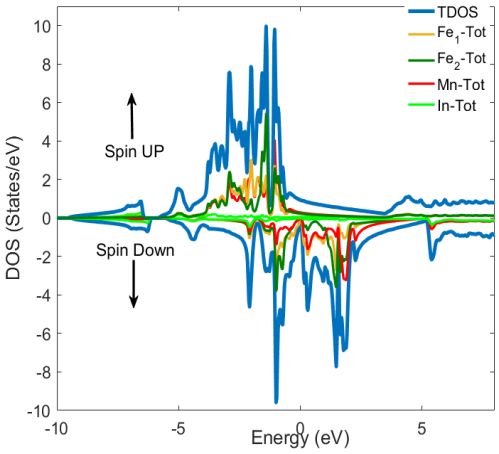

b

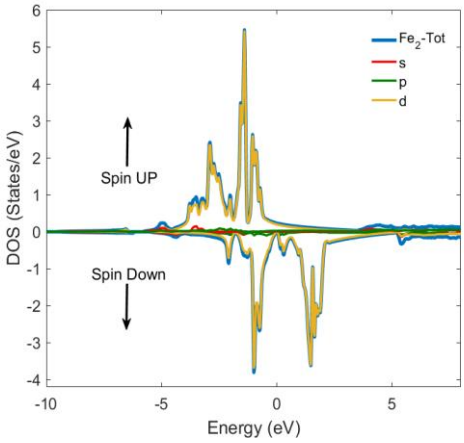

C

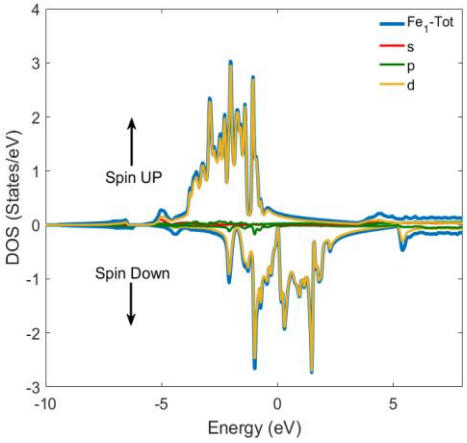

d

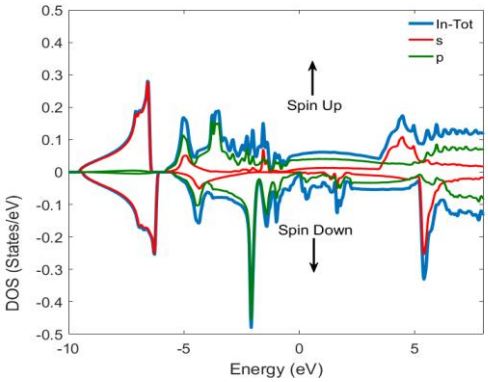

e

Note: (a) Total density of states (b) partial density of states of Fe1 atom(c)Fe2 atom (d)Mn atom (e)In atom.

Figure 18

Total and partial density of states of inverse Fe_2MnIn in spin up and spin down cases using mBJ-GGA

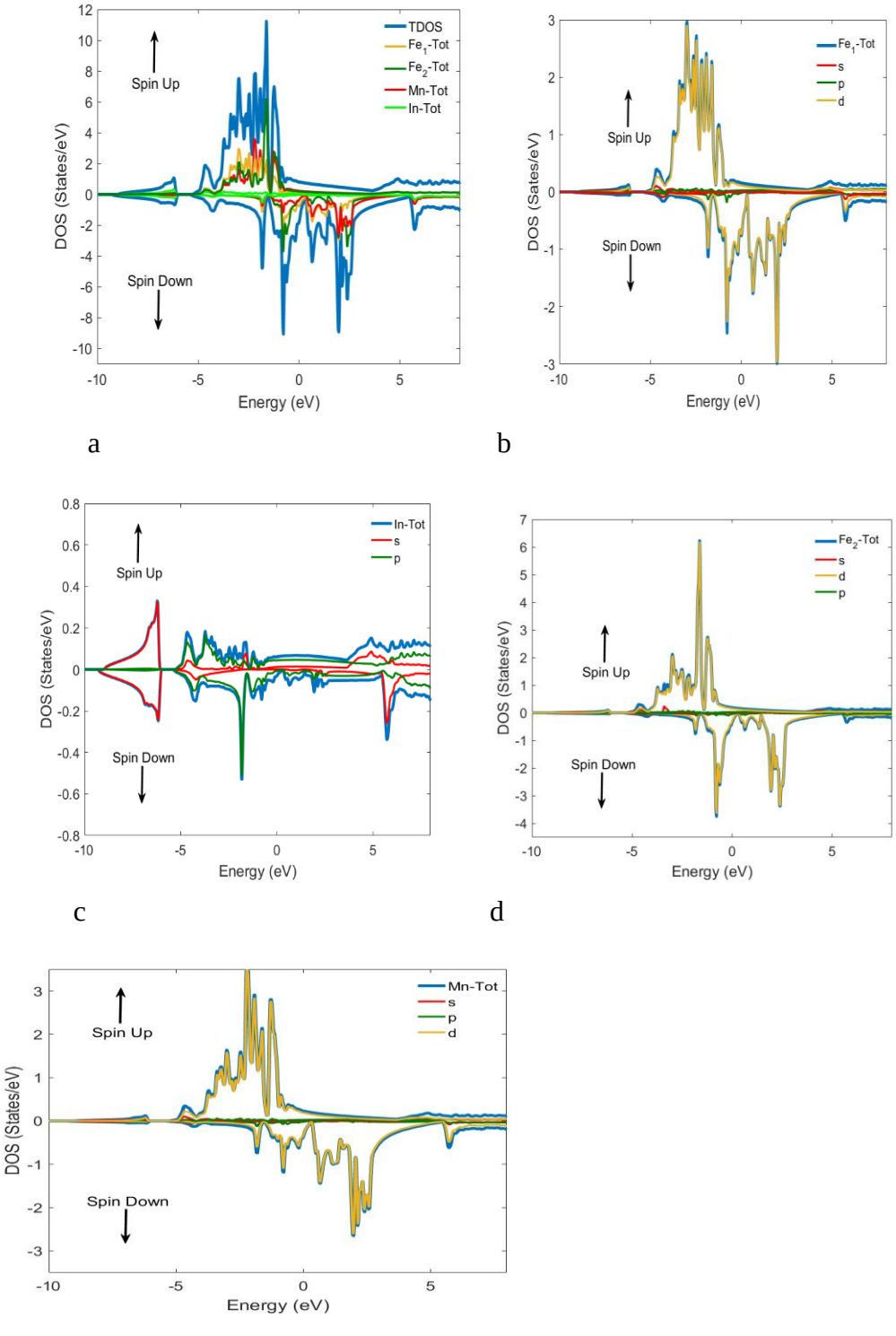

Note: (a) Total density of states (b) partial density of states of Fe1 atom(c)Fe2 atom (d)Mn atom (e)In atom.

جامعة النجاح الوطنية
كلية الدراسات العليا

الخصائص التركيبية، الإلكترونية، المغناطيسية، والمرونية لمركبات هزلر التامة بإستخدام طريقة الجهد التام Fe_2MnIn, Au_2MnIn

إعداد
سلمى نصر درويش بريك

إشراف
أ. د. محمد أبو جعفر
د. محمود القاروط

قدمت هذه الرسالة استكمالا لمتطلبات الحصول على درجة الماجستير في الفيزياء،
من كلية الدراسات العليا، في جامعة النجاح الوطنية، نابلس – فلسطين.

2024

الخصائص التركيبية، الإلكترونية، المغناطيسية، والمرونية لمركبات هزلر التامة بإستخدام طريقة الجهد التام Fe_2MnIn, Au_2MnIn

إعداد

سلمى نصر درويش بريك

إشراف

أ. د. محمد أبو جعفر

د. محمود القاروط

الملخص

لقد تمت دراسة الخصائص التركيبية، الإلكترونية، المغناطيسية والمرونية لمركبات (Fe_2MnIn and Au_2MnIn) هيزلر التامة بإستخدام طريقة الجهد التام المزيد ذو الموجات الخطية المستوية من خلال استخدام برنامج wien2K والقائم على نظرية الكثافة الوظيفية (DFT).

لقد تم حساب ثابت الشبكة ومعامل الصلابة ومشتقتها بالنسبة للضغط لمركبات (Fe_2MnIn and Au_2MnIn) من خلال استخدام التقريب التدريجي المعمم (GGA) وتحسين فجوة الطاقة بإستخدام جهد بيكي جونسون ، ومن ثم تم حساب الخصائص المغناطيسية والإلكترونية والمرونية.

ومن أبرز النتائج التي توصلنا إليها: تبين أن جميع المركبات لها خصائص مغناطيسية. وتبين ان المركب Fe_2MnIn العكسي له خصائص نصف معدنية. وتبين أن المركب Fe_2MnIn المنتظم و مركب Au_2MnIn المنتظم والعكسي تمتلك جميعها الخصائص المعدنية. وتبين أن المركبين Fe_2MnIn المنتظم و Au_2MnIn العكسي غير مستقرين ميكانيكياً. وتبين أن المركبين Fe_2MnIn العكسي و Au_2MnIn المنتظم مستقرين ميكانيكياً. وتبين أن المركبين Fe_2MnIn العكسي و Au_2MnIn المنتظم يمتلكان روابط أيونية. وتبين أن المركبين Fe_2MnIn العكسي و Au_2MnIn المنتظم لهما قابلية السحب والطرق.

الكلمات المفتاحية: مركبات هزلر التامة، فرومغناطيسية، المرونية، الإلكترونية، طريقة الجهد التام، نظرية الكثافة الوظيفية.